Palacký University Olomouc

Master thesis

Olomouc 2022 **Bc. Barbora Vrablíková**

Palacký University Olomouc

Faculty of Science

Department of Cell biology and Genetics

Analysis of cancer drug combination using 3D mono- and co-cultures of colorectal cell lines

Master thesis

Bc. Barbora Vrablíková

Study programme: Biology

Field of study: Molecular and cell biology

Form of study: Full time

Olomouc 2022

Supervisor: Mgr. Viswanath Das, Ph.D.

UNIVERZITA PALACKÉHO V OLOMOUCI

Přírodovědecká fakulta

Akademický rok: 2020/2021

ZADÁNÍ DIPLOMOVÉ PRÁCE

(projektu, uměleckého díla, uměleckého výkonu)

Jméno a příjmení:	Bc. Barbora VRABLÍKOVÁ
Osobní číslo:	R20916
Studijní program:	N1501 Biologie
Studijní obor:	Molekulární a buněčná biologie
Téma práce:	Analýza kombinace léků proti rakovině s využitím 3D mono- a ko-kultur kolorektálních buněčných linií
Zadávající katedra:	Katedra buněčné biologie a genetiky

Zásady pro vypracování

This study proposes to determine the potential of using 3D cell cultures for predicting drug synergy. The student will use mono- and co-cultures of HCT116 colorectal cancer cells and CCD-18Co normal colon fibroblasts to predict the effect of the combination of 3-4 selected drugs used in the clinic for the treatment of colon carcinoma. The effect of drugs will be determined by measuring the changes in spheroid size using microscopy and viability using CellTiter-Glo® 3D Cell Viability Assay Kit.

Rozsah pracovní zprávy:	
Rozsah grafických prací:	
Forma zpracování diplomové práce:	tištěná
Jazyk zpracování:	Angličtina

Seznam doporučené literatury:

1. Evelina Folkesson et al. (2020) High-throughput screening reveals higher synergistic effect of MEK inhibitor combinations in colon cancer spheroids. Scientific Reports volume 10, Article number: 11574 (2020).
2. Ravi S. Narayan et al. (2020). A cancer drug atlas enables synergistic targeting of independent drug vulnerabilities. Nature Communications volume 11, Article number: 2935 (2020).
3. V Das et al. (2016). Reproducibility of uniform spheroid formation in 384-well plates: the effect of medium evaporation. Journal of Biomolecular Screening. 21(9):923-30 (2016)

Vedoucí diplomové práce: Mgr. Viswanath Das, PhD.
Ústav molekulární a translační medicíny

Datum zadání diplomové práce: 29. října 2020
Termín odevzdání diplomové práce: 31. července 2022

UNIVERZITA PALACKÉHO V OLOMOUCI
PŘÍRODOVĚDECKÁ FAKULTA
KATEDRA BUNĚČNÉ BIOLOGIE A GENETIKY
Šlechtitelů 27, 783 71 Olomouc – Holice
tel.: +420 585 634 901
-2-

18 -03- 2022

L.S.

doc. RNDr. Martin Kubala, Ph.D.
děkan

prof. RNDr. Zdeněk Dvořák, DrSc.
vedoucí katedry

V Olomouci dne 18. března 2022

BIBLIOGRAPHICAL IDENTIFICATION

Author's name	Bc. Barbora Vrablíková
Title	Analysis of cancer drug combination using 3D mono- and co-cultures of colorectal cell lines
Type of thesis	Master
Department	Cell biology and genetics, Faculty of Science UP, Olomouc
Supervisor	Mgr. Viswanath Das, Ph.D.
The year of defense	2022

Summary

The synergistic interaction of anticancer drugs is an important part of cancer therapy. The combination of more than one drug in cancer therapy can have many advantages, including lower off-target effects, higher efficacy, and the potential to overcome or avoid the development of acquired resistance. Three-dimensional (3D) cell cultures, which effectively mimic tumor complexities, are becoming an important tool to accelerate translation research, cover shortcomings of 2D systems and better model drug delivery and drug-target interactions under physiological conditions. This study determined the potential of using 3D cell cultures for predicting drug synergy using mono- and co-cultures of HCT116 colorectal cancer cells and CCD-18Co normal colon fibroblasts to predict the effect of the combination of 3 selected drugs used in the clinic for the treatment of colon carcinoma. By measuring the changes in spheroid size using microscopy and viability using a 3D cell viability assay, the synergy relation of used drugs was confirmed in 3D cultures.

Keywords	colorectal carcinoma, 3D cultures, synergy, anticancer drugs
Number of pages	64
Number of appendices	0
Language	English

BIBLIOGRAFICKÉ ÚDAJE

Jméno autora	Bc. Barbora Vrablíková
Název práce	Analýza kombinace léků proti rakovině s využitím 3D mono- a ko-kultur kolorektálních buněčných linií
Typ práce	Diplomová
Pracoviště	Katedra buněčné biologie a genetiky, PřF UP v Olomouci
Vedoucí práce	Mgr. Viswanath Das, Ph.D.
Rok obhajoby práce	2022

Souhrn

Synergické působení protinádorových léčiv jsou důležitou součástí protinádorové terapie. Kombinace více než jednoho léku při léčbě rakoviny může mít mnoho výhod, včetně nižších vedlejších účinků, vyšší efektivity a schopnosti překonat získanou rezistenci nebo jí předcházet. Trojrozměrné (3D) buněčné kultury, které napodobují komplexnost nádorů, se stávají důležitým nástrojem pro translační výzkum a překonání nedostatků 2D systémů, mohou také lépe modelovat podávání léčiv a jejich cílení za fyziologických podmínek. V této studii byl zkoumán potenciál využití 3D buněčných kultur k predikci synergie pomocí monokultur a kokultur buněk kolorektálního karcinomu HCT116 a normálních fibroblastů tlustého střeva CCD-18Co k predikci účinku kombinace 3 vybraných léčiv používaných v klinické léčbě karcinomu tlustého střeva. Měřením změn velikosti sféroidů pomocí mikroskopie a viability pomocí testu životaschopnosti 3D buněk byl potvrzen vztah synergie použitých léčiv v 3D kulturách.

Klíčová slova	kolorektální karcinom, 3D kultury, synergie, protinádorová léčiva
Počet stran	64
Počet příloh	0
Jazyk	Anglický

DECLARATION

I declare, that this master thesis was written independently with help of my supervisor Mgr. Viswanath Das, Ph.D., and using the sources listed in the references.

In Olomouc, …… ……

Barbora Vrablíková

ACKNOWLEDGEMENT

I would like to thank my supervisor Mgr. Viswanath Das, Ph.D., for his support throughout the thesis, valuable advice, and trust he had in me. I appreciate his friendly and patient attitude, and I am grateful to him and Mgr. Narendran Annadurai. Both of them were always there for me, taught me new skills, and helped me throughout the work. Also, I would like to thank Mgr. Anna Janošťáková and Bc. Renata Buriánová for their friendly approach, support, and willingness to help and my family and friends for believing in me and supporting me during my studies.

CONTENT

ABBREVIATIONS

5-FU	5-fluorouracil
APC	Adenomatous polyposis coli
CI	Combination index
CIMP	CpG island methylator phenotype
CIN	Chromosomal instability
CPt	Cisplatin
CRC	Colorectal cancer
EGFR	Epidermal growth factor receptor
FAP	Familial adenomatous polyposis
HNPCC	Hereditary nonpolyposis colorectal cancer
IC_{50}	Half-maximal inhibitory concentration
IR	Irinotecan
KRAS	Kirsten rat sarcoma virus
MAPK	Mitogen-activated protein kinase
MMR	Mismatch repair gene
MSI	Microsatellite instability
TGF	Transforming growth fractor
TP53	Tumor protein p53
VEGF	Vascular endothelial growth factor

LIST OF FIGURES

LIST OF TABLES

1 INTRODUCTION

The synergistic interaction of anticancer drugs is an important part of cancer therapy. The combination of more than one drug in cancer therapy can have many advantages, including lower side effects, higher efficacy, or avoiding unwanted resistance. There are many methods for predicting drug synergy using two-dimensional (2D) cell cultures of cancer cell lines. 2D cancer cell cultures have a significant role in drug discovery and development; however, some limitations complicate further studies. Unfortunately, 2D-cellular models are not mimicking the physiology of tumors, whereas most new anticancer drugs fail in clinical trials, so it is important to find a better model for studying a new anticancer agent. Three-dimensional (3D) cell cultures can effectively mimic tumor complexities, thus becoming an essential tool for further research. 3D spheroids of cancer cells model the *in vivo* architecture of tumors, including multicellular arrangement, hypoxia, cell-cell interactions, and extracellular matrix deposition. Such arrangements, absent in 2D systems, can better model drug delivery and drug-target under physiological conditions.

This thesis will be focused on determining the potential of using 3D cell cultures for predicting drug synergy using mono- and co-cultures of HCT116 colorectal cancer cells and CCD-18Co normal colon fibroblasts to predict the effect of the combination of 3 selected drugs used in the clinic for the treatment of colon carcinoma.

2 AIMS OF THE THESIS

The first aim of the thesis was to prepare 3D mono- and co-cultures of colorectal carcinoma cell lines using agarose-coated 384-well plates. Monocultures consist of HCT116 colorectal carcinoma cells alone and co-cultures of HCT116 colorectal carcinoma cells with CCD-18Co normal colon fibroblasts at different cell number ratios.

The second aim was to treat prepared 3D cultures with three selected clinical oncology drugs alone and in combination and predict the synergistic activity by following changes in different parameters, such as spheroid size using microscopy and viability using CellTiter-Glo® 3D Cell Viability Assay.

3 LITERATURE REVIEW

3.1 Cancer global statistics

Cancer is the leading cause of death and shortening the length of life in the world (Jemal *et al*., 2011). According to a 2019 World Health Organization study, cancer is the leading cause of death in 112 of 183 nations, with cancer ranking as the first or second cause of death in these countries and third or fourth in 23 other countries. In 2020, there were 19.3 million new cases and 10 million cancer deaths worldwide (Sung *et al*., 2021) compared to 12.7 million new cases and 7.6 million cancer deaths globally in 2008 (Jemal *et al*., 2011).

Table 3.1: Global new cases, deaths and 5-year prevalence for different types of cancer in 2020 in both sexes (IARC, GLOBOCAN 2020).

	Incidence		**Deaths**		**5-year prevalence**	
Cancer	Number	(%)	Number	(%)	Number	Prop. (per 100 000)
Breast	2 261 419	11.7	684 996	6.9	7 790 717	201.58
Lung	2 206 771	11.4	1 796 144	18.0	2 604 791	33.42
Prostate	1 414 259	7.3	375 304	3.8	4 956 901	126.13
Colon	1 148 515	6.0	576 858	5.8	3 045 225	39.07
Stomach	1 089 103	5.6	768 793	7.7	1 805 968	23.17
Liver	905 677	4.7	830 180	8.3	994 539	12.76
Rectum	732 210	3.8	339 022	3.4	2 066 732	26.51
Cervix uteri	604 127	3.1	341 831	3.4	1 495 211	38.69
Oesophagus	604 100	3.1	544 076	5.5	666 388	8.55
Thyroid	586 202	3.0	43 646	0.44	1 984 927	25.46

According to GLOBOCAN, there were 519,820 new cases of colorectal cancer (CRC) in Europe in 2020. This number makes CRC the second most common cancer in Europe (Ferlay *et al.*, 2021). The increased CRC cases in Europe most likely reflect lifestyle factors, such as diets rich in meat, sedentary life and higher body weight, or other factors – smoking cigarettes, heavy alcohol consumption, and others (Sung *et al.*, 2021).

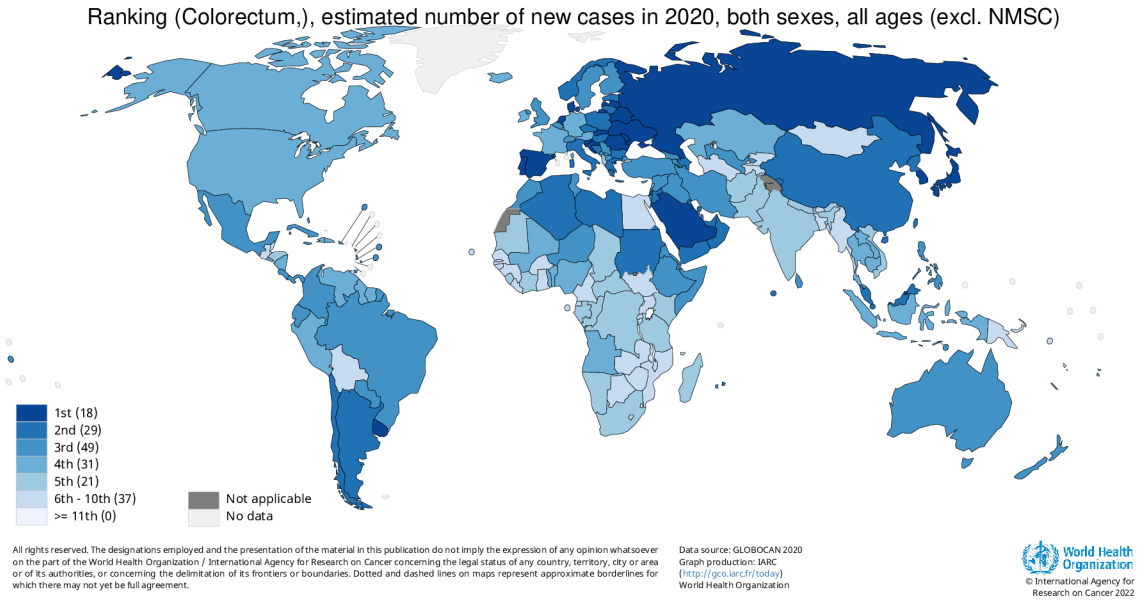

Figure 3.1: Incidence of colorectal carcinoma worldwide in both sexes. Dark blue indicated the highest number of new cases, and light blue the lowest number of new cases. The Czech Republic is the second in the rating (Source: GLOBOCAN 2020).

3.2 Etiology of CRC

Different mutations of specific oncogenes, tumor suppressor genes, genes related to DNA reparations, and others lead to the development of a wide range of cancer, including CRC. However, CRC can be sporadic, familial, or inherited according to the origin of the mutation (Fearon *et* Vogelstein, 1990). Approximately 25 % of CRC patients have a familial background, and 5 % of CRC is caused by single-gene syndromes, such as adenomatous polyposis (FAP) or Lynch syndrome, known as hereditary nonpolyposis colorectal cancer (HNPCC) (Arnold *et al.*, 2005; Fearon et Vogelstein, 1990). In fact, 70 % of CRC is caused by point mutations, which affect only individuals, and the effects are not hereditary. This is a sporadic type of cancer, and mutations can

change different genes, and it is usually a multistep process (Fearon *et* Vogelstein, 1990). The beginning of the sporadic type of CRC is caused by mutations in the tumor suppressor gene, adenomatous polyposis coli (*APC*) in epithelial tissue, leading to polyps formation, which are non-malignant. About 15 % of these non-malignant adenomas transform to carcinoma in the next 10 years, with additional mutations in genes, such as Kirsten rat sarcoma viral oncogene (*KRAS*), tumor protein p53 (*TP53*) and deleted in colorectal cancer (*DCC*) (Arnold *et al*., 2005; Mármol *et al*., 2017).

3.2.1 Molecular insight into CRC

The development of CRC precedes a cumulative process of sequential genetic alternations (Arnold *et al*., 2005). These alternations include mutations, translocations, and chromosomal changes in essential pathways such as WNT, MAPK/PI3K, TGF-β, TP53 and mutations in common genes such as *c-MYC*, *KRAS*, *BRAF*, *PIK3CA*, *PTEN*, or *SMAD2* and *SMAD4* (Fearon, 1995; Pino *et* Chung, 2010).

The genomic instability which leads to CRC comprises chromosomal instability (CIN), microsatellite instability (MSI) and CpG island methylator phenotype (CIMP), with the CIN pathway present in up to 85 % of CRC cases (Agrawal *et al*., 2018; Grady *et al*., 2008). CIN pathway leads to aneuploid tumors and lack of heterozygosity (LOH) because of deviations in chromosome number, leading to telomere dysfunction, instability in chromosome segregation and DNA damage response, influencing essential genes such as *KRAS*, *APC*, *PI3K, TP53* and others. If there is a mutation in *KRAS* or *PI3K*, MAP-kinase is constantly active, increasing cell proliferation. Mutations in the *TP53* gene encoding p53 causes the disrupted cell-cycle checkpoint, and mutations in the *APC* cause translocation of β-catenin to the nucleus, following transcription of genes supporting tumor growth and invasion (Pino *et* Chung, 2010).

In the case of microsatellite instability, loss of DNA repair mechanisms, such as mismatch repair gene (*MMR*), causes accumulation of mutations in tandem repeats of short DNA chains, affecting the non-coding regions and codifying microsatellites, which leads to tumor development. Thus, microsatellite instability is caused by hypermutable phenotype, whereas mutations in these tumor types include

genes such as *MLH1*, *MSH2*, *MSH6*, *PMS1* and *PM2*. MSI tumors, however, have a better prognosis than sporadic tumors (Boland *et* Goel, 2010).

The third instability responsible for CRC is CpG island methylator phenotype, characterized by hypermethylation of oncogene promoters. This leads to protein expression loss and genetic silencing (Lao *et* Grady, 2011; Agrawal *et al*., 2018).

3.2.2 Current treatment of CRC

The treatment of colorectal carcinoma depends on tumor characteristics such as its progression, number and localization of metastases and others. Resection of tumor is often accompanied by chemotherapy and radiotherapy, whereas their combination is proved to be more effective than alone (Sauer *et al*., 2004). Chemotherapy is significant in treating metastatic tumors, despite drug resistance and side effects. Most CRC patients are treated with cytotoxic and targeted biology agents, depending on the patients' genotype (Mármol *et al*., 2017).

The most used single-agent chemotherapeutics for treating CRC are 5-fluorouracil, leucovorin, oxaliplatin and irinotecan, but the combination of these drugs showed greater efficacy than the use of drugs alone. The first-line chemotherapy includes 5-fluorouracil and capecitabine alone or combined with leucovorin or oxaliplatin (Goldberg *et al*., 2004). There are multiple combinations of different drugs in the treatment of CRC, such as 5-fluorouracil, and leucovorin together with oxaliplatin, called FOLFOX (Shi *et al*., 2012), CAPOX, which is a combination of capecitabine, leucovorin and oxaliplatin. The use of leucovorin in these combinations reduces the cytotoxicity of treatment (Hirsch *et* Zafar, 2011). CRC patients are also treated with irinotecan if the first-line treatment is intensified. Irinotecan is also used to treat pancreatic, ovarian, cervical, and gastric cancers. Its mechanism is based on substrate competition and interactions between protein and DNA (Mármol *et al*., 2017). Cisplatin is one of the most efficient agents in cancer therapy. Its cytotoxicity results in DNA-platinum formation, and when combined with 5-fluorouracil and other drugs, it shows potency anticancer effects (Dasari *et* Tchounwou, 2014; Agrawal *et al*., 2018).

3.2.3 Targeted therapy

To improve the outcome of CRC therapy, patients are given monoclonal antibodies, proteins against vascular endothelial growth factor (VEGF) or epidermal growth receptor (EGFR). The most commonly used monoclonal antibodies against VEGF-A are Bevacizumab and Aflibercept, which block VEGF-B or growth factors from placenta. Cetoximab and Panitumumab target EGFR (Cutsem *et al.*, 2014).

3.2.4 Drug-drug interaction

The combination of different drugs is extensively used to treat different diseases, particularly cancer (Chou, 2006). Two or more drugs can interact with each other differently, and this can be distinguished into three interactions – synergistic, additive, or antagonistic. The evaluation of the relation between two drugs is important for further use, and this is defined by the scientific term "combination index" (CI). A synergy between drugs is seen when the CI value is < 1, additive effect when the CI value = 1, and antagonism when the CI is > 1 (Chou *et* Talalay, 1983).

The combination index (CI) is calculated by Eq. 1 (Zhao *et al.*, 2010).

$$CI = \frac{C_{A,x}}{IC_{x,A}} + \frac{C_{B,x}}{IC_{x,B}}$$

There are various reference models in pharmacodynamics that are used to characterize the relationship between two drugs. The most commonly used model is Loewe additivity, or also dose additivity. This analysis defines the interaction between drug A and drug B at a given effect level (Zhao *et al.*, 2010). It is necessary to obtain a concentration required for cell inhibition, so the synergism is a question of doses of each drug in combination; thus, the most used maximum concentration in studies is often the concentration that provides 50 % of the effect (e.g., IC_{50}) of each drug A (ICx, A) and B (ICx, B) (Tallarida, 2012). These concentrations are indicated on a two-coordinated plot's x and y axes, and two points (ICx, A, 0) and (ICx, B, 0)

are formed. The additivity relation of the two drugs is displayed as a line connecting these two points. After performing the combinations of two drugs, these concentrations are placed in the same plot. Relation between two drugs is determined according to the location of concentration, i.e., if it is below, on or above the line (Chou, 2010; Zhao *et al*., 2010).

The synergism simplifies cancer treatment which must deal with resistance caused by genetic and phenotypic heterogeneity of cancer and high toxic concentration of anticancer agents (Greco *et al*., 1995). Heterogeneity between tumors makes the prediction of treatment among patients challenging (Palmer *et al*., 2017). Also, it helps to obtain better efficacy against tumor, without using higher concentrations which can cause more side effects and create an obstacle in cancer treatment (Greco *et al*., 1995). For successful treatment, it is necessary to obtain at least the best response for one of the two used drugs; however, their combinations should implement even better results due to each other's drawback compensation, that is why it is important to study more drug synergies to obtain better results in cancer treatment (Palmer *et al*., 2017).

Since gene expression patterns of 3D cultures are closer to *in vivo* growth environment of tumors than in 2D, this model can provide more accurate data about drug treatment, drug combinations, and synergistic effects of different drugs and to discover new mechanisms and targets. Various parameters can be measured and comples data can be obtained using mono- or co-cultures and studying differences between effects of used drug combinations (Folkesson *et al*., 2020; Foglietta *et al*., 2021).

3.3 Cell culture models

Cultures of cancer cell lines are important *in vitro* models in cancer treatment research for discovering different drug responses, stem cell studies, etc. Two-dimensional cell cultivation is a routine method used in laboratories around the world. However, the fact that 2D-cellular models cannot mimic the microenvironment of solid tumors, limits their application in several studies (Hayhock, 2011). Around 95 % of new anticancer drugs are reported to fail in clinical trials, making it important to find better *in vitro* tumor models for preclinical research (Hickman *et al.*, 2014). An important property of tumors and tissues is that the cells grow in three dimensions, so it is more relevant to use three-dimensional (3D) cell models for testing the efficacy of potential drugs at an early phase of drug discovery research (Hayhock, 2011; Hickman *et al.*, 2014). With 3D cell models, it is possible to provide more precise data about tumor characterization, cell-cell interactions, metabolic profile, stem cell research and tumor cell response to therapies (Jensen *et* Teng, 2020).

3.3.1 Two-dimensional cellular models

Cell cultivation in two dimensions has been a standard method used since the 1900s (Ferreira *et al.*, 2018). More precisely, Ross Granville Harrison invented the technique in 1907, following his research on the origin of nerve fibres from frog embryos (Breslin *et* O'Driscoll, 2012). In the 1950s, a potential drug screening method was introduced using cells cultivated in glass flasks in a semisynthetic medium. The correlation between *in vitro* cell cultures and clinical responses to a drug was very faint. Another milestone was inventing a colony-forming assay by Hamburger and Salmon in the 1970s. This method allowed growing isolated fresh human material as a single-cell solution on soft agarose. However, this assay was also considered as not very efficient due to the requirement of a constant supply of fresh human material, which complicated the screening of a broader range of different compounds and limited the success of *in vitro* studies to predict the sensitivity of patients' tumor to clinically approved drugs (Hickman *et al.*, 2014).

However, many improvements have been made, from using a synthetic medium, which brings many advantages, such as the absence of antigens, low price, and presence

of antibiotics, to easy growth of cell lines on a flat surface and their manipulation. The 2D culturing is still developing, but a correlation of results from 2D cultures and *in vivo* animal studies is poor (Breslin *et* O'Driscoll, 2012). Some of the major issues currently encountered with 2D cultures include a low number of cell-cell and cell-stroma interactions and no replication of tumor heterogeneity or the genetic profile of original tissue. On the other hand, the low cost, easy handling, compatibility with imaging and other systems, and a large number of available data on 2D cultures make them favorable models (Das *et al*., 2015; Zanoni *et al*., 2016).

3.3.2 Three-dimensional cellular models

Since results of 2D cultures treatment have a poor correlation with clinical data, a new dimension was added for improving a drug discovery by growing cells in a 3D environment that reproduces the natural growth condition of all cell types (Breslin *et* O'Driscoll, 2012).

3D tumor spheroids of cancer cells show different zones of necrotic and hypoxic parts, which arise due to the limited diffusion of nutrients and oxygen (Figure 3.2) (Hirschhaeuser *et al*., 2010). The outer layer of spheroids is composed of proliferating cells in the G_2/M phase of the cell cycle, whereas the core of spheroids displays a highly hypoxic environment with cells arrested in the G_1 phase (Laurent *et al*., 2013).

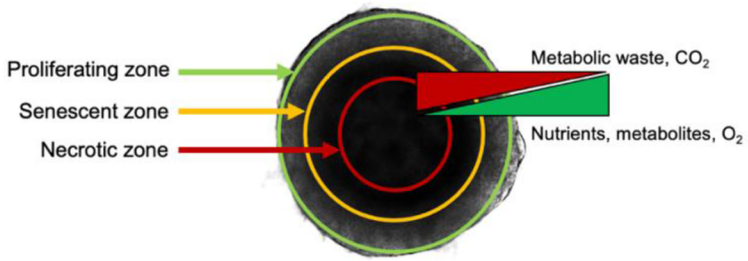

Figure 3.2: Brightfield image of HCT116 spherical colony and their structure. The outer layer of a spheroid, proliferating zone, is rich in oxygen with cells in the G2/M phase. The inner layer, the senescent zone, is made by cells in the G1 phase, and finally, the inner necrotic zone is composed of hypoxic necrotic cells. The center of the spheroid shows high levels of CO_2 and metabolic waste due to the diffusion gradient, whereas the outer zone shows high levels of nutrients, metabolites, and oxygen.

Three-dimensional cellular cultures can be scaffold-free or scaffold-based. Different 3D cellular models include microcarrier cultures, tissue-engineered models, and animal and organotypic explant cultures, including embryos and patient-derived tumor cell organoids. Cellular spheroids are 3D models that can be self-assembled from different cell types using various methods. Mono- or co-culture spheroids using non-adherent techniques do not require scaffolds as necessary for other 3D culture models. The spheroids formed can be easily imaged by light, fluorescent, confocal and light-sheet microscopes, making them relatively easy and cost-effective 3D cellular models for different studies, such as drug response, tumor cell metastasis or solid tumor growth (Hayhock, 2011).

3.3.3 Methods of spheroid formation

There are a variety of non-scaffold methods for spheroid formation, including the hanging drop method, magnetic levitation, and forced floating, each with its own set of benefits (Breslin *et* O'Driscoll, 2012; Ferreira *et al.*, 2018). Hanging drop in microplates uses gravity to form spheroids, and it is affordable if using 96-well plates. Spheroids are accessible and homogenous, so it is suitable for further high-throughput testing. The disadvantage of this system is the difficulty of changing media in small culture volumes and plate preparation itself (Breslin *et* O'Driscoll, 2012). Magnetic levitation uses magnetic nanoparticles, which are introduced into cells first and, after magnet exposure, result in spheroids.

However, the most common method for 3D cell model formation is spheroid microplates with a non-adherent surface, which is straightforward and suitable for high-throughput screening as spheroids are easily accessible and can be formed in different sized spheroids by determining the number of cells. This method is straightforward but sensitive to human error while exchanging media, and cell seeding; however, this can be overcome by using automatized methods. Another disadvantage is the high price of commercial plates with a non-adherent surface; however, this can be replaced by agarose-based plates, which are relatively inexpensive and suitable in 96- or 384- well plates format (Breslin *et* O'Driscoll, 2012; Das *et al.*, 2015).

For more complex studies, scaffolds or matrices can be used; however, different scaffolds are needed for different cell types, and their disruption or break must not be toxic to cells (Hayhock, 2011). The use of scaffold is included in microfluidic cell culture platforms, which are very suitable for high-throughput testing, but hardly represent *in vivo* environment. The disadvantage of matrices and scaffolds is their price in the large-scale production and retrieving of cells following 3D culture formation for downstream analysis (Breslin *et* O'Driscoll, 2012).

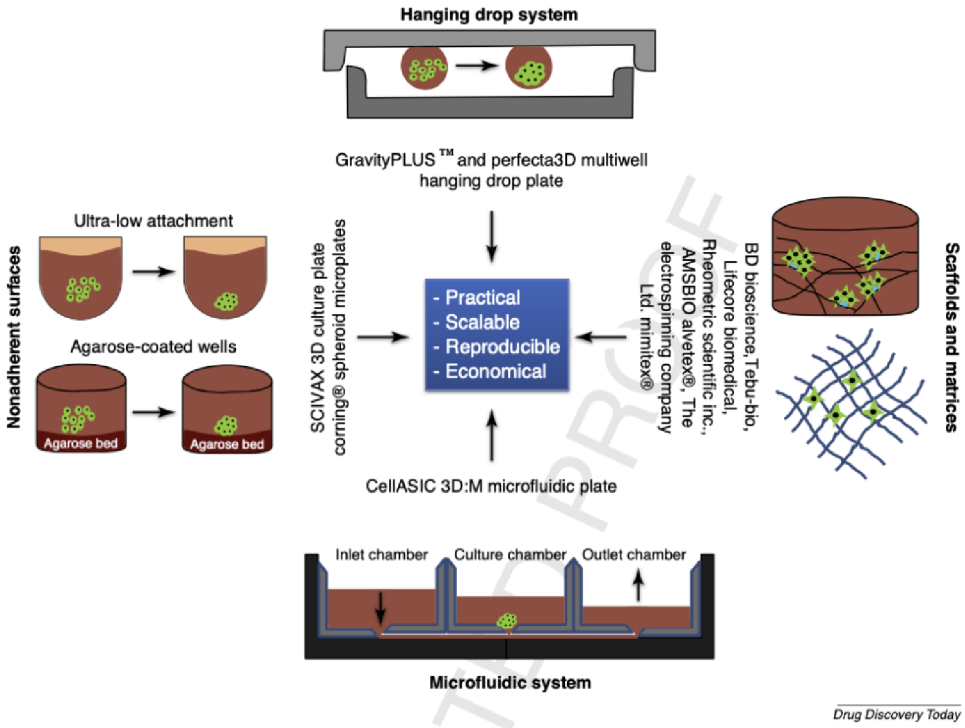

Figure 3.3: Different methods commonly used for 3D cell culture preparation, including Hanging drop system, Scaffold and matrices, Microfluidic system and Forced floating system, and Non-adherent surfaces (Das *et al*., 2015)

3.3.4 Differences between 2D and 3D cell culture models

3D models bring many benefits over 2D cell cultures, including a gradient of oxygen and nutrients, significant histological morphology of different tumors and alternations of the cell cycle in microregions of tumors, which can be caused by the hypoxic environment (Das *et al*., 2015). Since 2D cultures are more susceptible

to the drugs because of their growth in monolayer, 3D cultures would be able to predict drug response more accurately due to the differences in the diffusion of drugs through different layers and regions of cells, thus mimicking drug diffusion in solid tumors (Cushing *et* Anseth, 2007). Additionally, 2D cells have a different distribution of cell surface receptors, which can also alter the activity of drugs (Bonnans *et al.*, 2014; Lv *et al.*, 2016).

Another important difference is that 2D cells are usually presented in the same cell cycle stage, whereas the cell cycle in 3D cultures differs, corresponding to *in vivo* tumor cells (Langhans, 2018). That means that there are proliferating cells in the outer region of spheroids, which could be important for an effective response to mitotic drugs (Bonnans *et al.*, 2014; Langhans, 2018).

Finally, the local pH levels differs in 2D and 3D culture cells. Different stages of the cell cycle, regions of hypoxia, acidity and necrotic core can cause a lower uptake and accumulation of weakly basic anticancer drugs. The amended pH levels induced by insufficient oxygen inside the tumour lead to hypoxia, lactic acid production, and ATP hydrolysis. Deficiency of ATP caused by hypoxia results in failure of Na^+ and K^+ gradient, membrane depolarization, and increased cytosolic Ca^{2+} levels, which leads to tumor acidosis and other issues (Das *et al.*, 2015). Thus 3D cultures may provide a better system to test the intracellular accumulation of these drugs in cells in different regions of spheroids (Lancaster *et* Knoblich, 2014). The extracellular microenvironment of tumors also consists of stromal cells (fibroblast and inflammatory cells), leading to resistance to anticancer treatment (Straussman *et al.*, 2012). However, despite many benefits, some shortcomings affect the use of 3D cultures regularly (see Table 3.2).

Table 3.2: Advantages and disadvantages of 2D and 3D cultures for studying the effects of anticancer drugs (Das *et al*., 2015; Jensen *et* Teng, 2020)

Method	Advantages	Disadvantages
2D cultures	Easy to culture and image Suitable for different assays Affordable Many 2D data available because of high replicability and easy interpretation	Few cell-cell and cell-stroma interactions Genetic profile differs to the origin of tissue Without histological morphology of the tumor of origin
3D culture	Mimic tumor microenvironment Oxygen and nutrient gradient of tumors Cell cycle alterations induced by hypoxia Good drug metabolism and more accurate representation of drug effects Protein and gene expression is very similar to *in vivo* cells	Complex assays and replication of experiments Absence of tumor vasculature More expensive HTS compatibility is still developing Need for higher drug concentrations and are more likely to be resistant to drug treatment

4 MATERIALS AND METHODS

4.1 Biological material

In this thesis, human carcinoma cell lines, colorectal cancer HCT116 cells stably expressing green fluorescent protein (GFP), and human normal colon cell line, CCD-18Co, which exhibits fibroblast-like morphology. All cell types were purchased from ATCC (Manassas, VA, USA). HCT116 cells, stably expressing GFP, were obtained from the Tissue Bank of the Laboratory of Experimental Medicine of the Institute of Molecular and Translational Medicine. HCT116 cells were cultivated in McCoy's 5A media with L-glutamine supplemented with 10% FBS and 1% Penicillin-Streptomycin. CCD-18Co cells were cultivated in Minimum Essential Medium (MEM) with Earle's Balanced Salts (MEM Eagle EBSS) without L-Glutamine supplemented with 10% FBS and 1% Penicillin-Streptomycin. Cells were cultured in a humified 5% CO_2/atmospheric air incubator at 37 °C.

4.2 Chemicals and reagents

- CellTiter-Glo® Cell Viability Assay (Promega, Cat. no. G9681)
- Eagle with Earle's BSS (MEM Eagle EBSS) without L-Glutamine (Lonza, Cat. no. 12-125Q)
- Fetal bovine serum (FBS; Gibco, Thermo Fisher Scientific, Inc., Cat. no. 10270106)
- jetPrime® transfection kit (Polypus transfection, Cat. no. 114-15)
- Low-melting agarose (Sigma-Aldrich, Cat. no. A9414)
- McCoy's 5A media with L-glutamine (Lonza, Cat. no. 12-688F)
- Penicillin-Streptomycin (Gibco, Thermo Fisher Scientific, Inc, Cat. no. 15140122)
- TrypLE™ Express Enzyme (1X), no phenol red (Thermo Fisher Scientific, Cat. no. 12604013)

4.3 Drugs

- 5-fluorouracil (Hospira UK Limited, United Kingdom)
- Cisplatin (Ebewe Pharma, Austria)
- Irinotecan (Pfizer spol. s.r.o., Czechia)

4.4 List of equipment

- –80 °C freezer
- 96-well (TPP) and 368-well cell culture-treated plates (PerkinElmer)
- Automatic pipetting filler Pipetus® (Hirschmann TM)
- Axio Observer D1 Fluorescent microscope (Carl Zeiss)
- Benchtop Centrifuge 5810R (Eppendorf centrifuge)
- Enspire Multimode Plate reader 2300-001M (Perkin Elmer)
- Eppendorf pipettes (0.5–1000 µl)
- FastGene Mini Centrifuge (Nippon Genetics)
- Heracell™ VIOS incubator (ThermoFisher Scientific™)
- Laminar flowbox MSC-Advantage™ Class II Biological Safety Cabinet (ThermoFisher Scientific™)
- Olympus IX51 Inverted Phase Contrast Fluorescence Microscope (Olympus)
- Rotina 420R Centrifuge (Hettich Zentrifugen)
- ViCell™ XR Cell Viability Analyzer (Beckman Coulter)
- Vortex V-1 Plus (Biosan)
- White Opaque 96-well and 384-well OptiPlate™ microplates (PerkinElmer)

4.5 Experimental and evaluation procedures

4.5.1 Cell cultivation

Cell lines were cultivated in T-75 cell culture-treated flasks with an appropriate medium, passaged 2–3 times a week and regularly tested for mycoplasma and bacterial contaminations following the standard protocols of the Laboratory of Experimental Medicine of the Institute of Molecular and Translational Medicine. Cells were observed under a microscope to check if the cell population reached 80% confluency before using

cells for experiments. For passaging, cells were washed twice with 1× PBS to remove the remaining medium and dead cells and treated for 2 minutes at 37 °C with TrypLE to facilitate cell detachment. To inactivate TrypLE, complete growth media was added to the flask and cells were transferred to a colonial-bottom 15-ml Falcon tube for centrifugation at 300 x g for 5 minutes. The cell pellet was resuspended in 5 ml of media, and 0.5 ml of suspension was used to measure cell number and viability using a ViCell Automated Cell Counter.

4.5.2 Cell transfection and transduction

CCD-18Co cells were transduced with Plenti-CMV-MCS-RFP-SV-puro particles. To produce lentiviral particles, 15 x 10^6 HEK 293T/17 cells were plated per 75 cm^2 flask and allowed to reach 80–90% confluency. For transfection of one 75 cm^2 flask of HEK 293T/17 cells, a transfection mixture of plasmid vectors was prepared according to Table 4.1 described below in 1.5 ml of jetPrime buffer supplemented with 90 µL jetPrime reagent, and following the manufacturer's protocol.

Table 4.1: Vectors used for the transfection of HEK 293T/17 cells.

Vector name	Vector size (bp)	Moles of DNA	DNA amount (µg) in 75 cm^2 flask
pMD2G	5 824	1.528 pmol	5.5
psPAX2	10 668	1.517 pmol	10
Plenti-CMV-MCS-RFP-SV-puro	8 411	1.539 pmol	8

Prior to adding the transfection mixture to cells, the old medium from the flask was replaced with 15 ml of fresh complete growth medium. The transfection mixture was added to the flask, and the cells were incubated for 16 hours. The old medium was replaced with 20 mL of complete fresh media the following day. Viral production was allowed to continue for the next 72 hours post-transfection of HEK 293T/17 cells before harvest (about 100% confluent in 3 days). The medium was

depleted by 72 hours. Cells producing viruses have a distinct rounded phenotype. After 72 hours, the medium was collected in a Falcon tube and centrifuge for 5 minutes at 1 500 rpm. The supernatant was filtered through a 0.45-µm filter using a 20 mL syringe. Next, the old medium from the flask containing CCD-18Co cells was removed and replaced with the lentiviral particle-containing filtered supernatant, supplemented with 8 µm/ml polybrene. The next day, the medium was changed, and lentiviral transduction of CCD-18Co cells was confirmed by the expression of dsRed2 using fluorescence microscopy after 48 hours.

4.5.3 Generation of spheroids using agarose coated plates

Plates were prepared according to the protocol of Das *et al.*, 2016. Plates were coated with 0.75% (w/v) low-melting agarose dissolved in McCoy's 5A medium without FBS or antibiotic supplements, boiled using a microwave oven to dissolve the low-gelling temperature agarose and autoclaved to sterilize. The 384-well plates were coated with 15 µl of 0.75% agarose under sterile conditions using an automated liquid dispenser as described in Das *et al.*, 2016. The coated plates were stored at 4 °C for further use.

Before use, plates were equilibrated to room temperature. Cells were seeded at a density 10 000 cells/ml (5 000 cells/well) to produce monoculture spheroids of HCT116 cells. HCT116 and CCD-18Co cells were seeded per well at 3:7 and 7:3 (HCT116:CCD-18Co) ratios to generate co-culture spheroids. The total cell number for co-culture spheroids was always 5 000 cells/well. Following cell seeding, the plate was allowed to rest for 30 minutes and then centrifuged at 4 x g for 20 minutes at room temperature. Next, the plate was replaced in a 37 °C standard incubator for 3 days to allow cells to aggregate into spheroids. The medium was replaced every 3 days, and spheroids were treated with selected drugs. Spheroids were imaged before and after 3 and 7 days of treatment using a fluorescent microscope (Carl Zeiss Axio Observer D1). The spheroid size and fluorescence change were recorded using Carl Zeiss ZEN 3.2 (Blue edition) software.

4.5.4 Cell viability assay

For determining spheroid viability, CellTiter-Glo® 3D Cell Viability Assay, based on luciferase reaction, was used. Used reagent results in cell lysis and generates a luminescent signal proportional to the amount of ATP, corresponding to the number of viable cells in culture. The relation between the number of cells and luminescence signal in 3D cultures is often curvilinear due to contact inhibition effects on cell proliferation, reduced metabolic activity and necrosis in the centre of the spheroid.

Before using the CellTiter-Glo® 3D Cell Viability Assay reagent, it was important to equilibrate the reagent in a 22 °C water bath for 30 minutes. First, an ATP standard curve was generated, which confirms if the luminescence of the 3D cell culture method is under the 10-µM limit. Cells were seeded at different numbers ranging from 1000 cells/well to 10 000 cells/well. Each well contained 100 µl of media. The next day, 50 µl of media was removed, and 50 µl of CellTiter-Glo® 3D Cell Viability Assay reagent was added. Plates were shaken for 5 minutes and incubated for 25 minutes to stabilize the luminescent signal. After incubation, an appropriate volume of the content of the wells was transferred to a white opaque 96-well microplate, and the luminescence signal was recorded using an EnSpire Plate Reader.

Plates with spheroids were equilibrated to room temperature for 30 minutes, and 25 µl of media was removed from each well and added to 25 µl of CellTiter-Glo® 3D Cell Viability Assay reagent. The content of the wells was mixed for 5 minutes and incubated for additional 25 minutes at room temperature. After incubation, the luminescence signal was recorded using the EnSpire Plate Reader, and the IC_{50} values of drugs were determined from their respective dose-response curves using GraphPad Prism (GraphPad Software, San Diego, CA)

4.5.5 Synergy studies

Cells were treated with individual drugs or a combination of two drugs for 7 days. To construct a concentration-response curve for individual medications, spheroids were treated with 1, 20, 50 and 100 µM of each drug, and their concentrations in combination were chosen based on individual IC_{50} values of the compounds. There were 5 different

combination concentrations chosen for each drug pair – 4:1, 2:1, 1:1, 1:2, 1:4, 5-FU and CPt or IR and CPt, and at least 3 biological replicates were performed. The combination doses were lower than the IC_{50} values for each agent alone, as it has been discovered that levels over the IC_{50} do not synergize. Drug combinations can have an antagonistic effect (drugs compete with one another and reduce their respective potencies), an additive effect (the combined effect is the sum of the singular effects of the two drugs), or a synergistic effect (an effect more significant than the sum of the drugs individual effects). The combination index (CI) for synergy was calculated using CompuSyn 1.0 as described by Chou *et al*., when synergy between drugs is when the CI value is < 1, additive effect when the CI value = 1, and antagonism when the CI is > 1 (Chou *et* Talalay, 1983).

4.5.6 Image processing, data analysis, and final compilation

For editing and exporting images, the following were used:

- Carl Zeiss ZEN 3.2 (Blue edition)
- ImageJ ver. 1.52a
- Microsoft PowerPoint ver. 16.37
- Inkscape ver. 0.92

For data analysis, the following software was used:

- CompuSyn 1.0
- GraphPad Prism 8
- Microsoft Excel ver. 16.37

5 RESULTS

5.1 Preparation of 3D cell using agarose-coated plates

It was important to prepare spheroids of uniform size to study cell responses to different drug treatments. To prepare 3D cell cultures, cells were seeded in agarose-coated plates at the density 5 000 cells/well according to the protocol described in Chapter 4.5.3. Approximately one day after seeding, cells started to aggregate into spheroids. These spheroids were imaged on days 3, 6 and 10 of cultivation to measure their size (Figure 5.1).

On day 3, HCT116 3D monocultures showed greater size than HCT116 and CCD-18Co cocultures, possibly due to their faster growth. On day 10, monocultures and cocultures grew about a third of their size, as seen in Figure 5.1. The final maximal size of spheroids was ~300–400 µm. In addition to the morphological changes (size), spheroids were imaged by fluorescent microscope to measure changes in the fluorescence signal with spheroid growth - green signal for HCT116 cells and red signal for CCD-18Co cells. As shown in Figure 5.2, CCD-18Co normal colon cells in cocultures were localized in the spheroid centre. Due to the optimal limit of the fluorescence microscope, the location of CCD-18Co cells in the spheroid centre was not visible in larger sized coculture spheroids on days 6 and 10 (Figure 5.2).

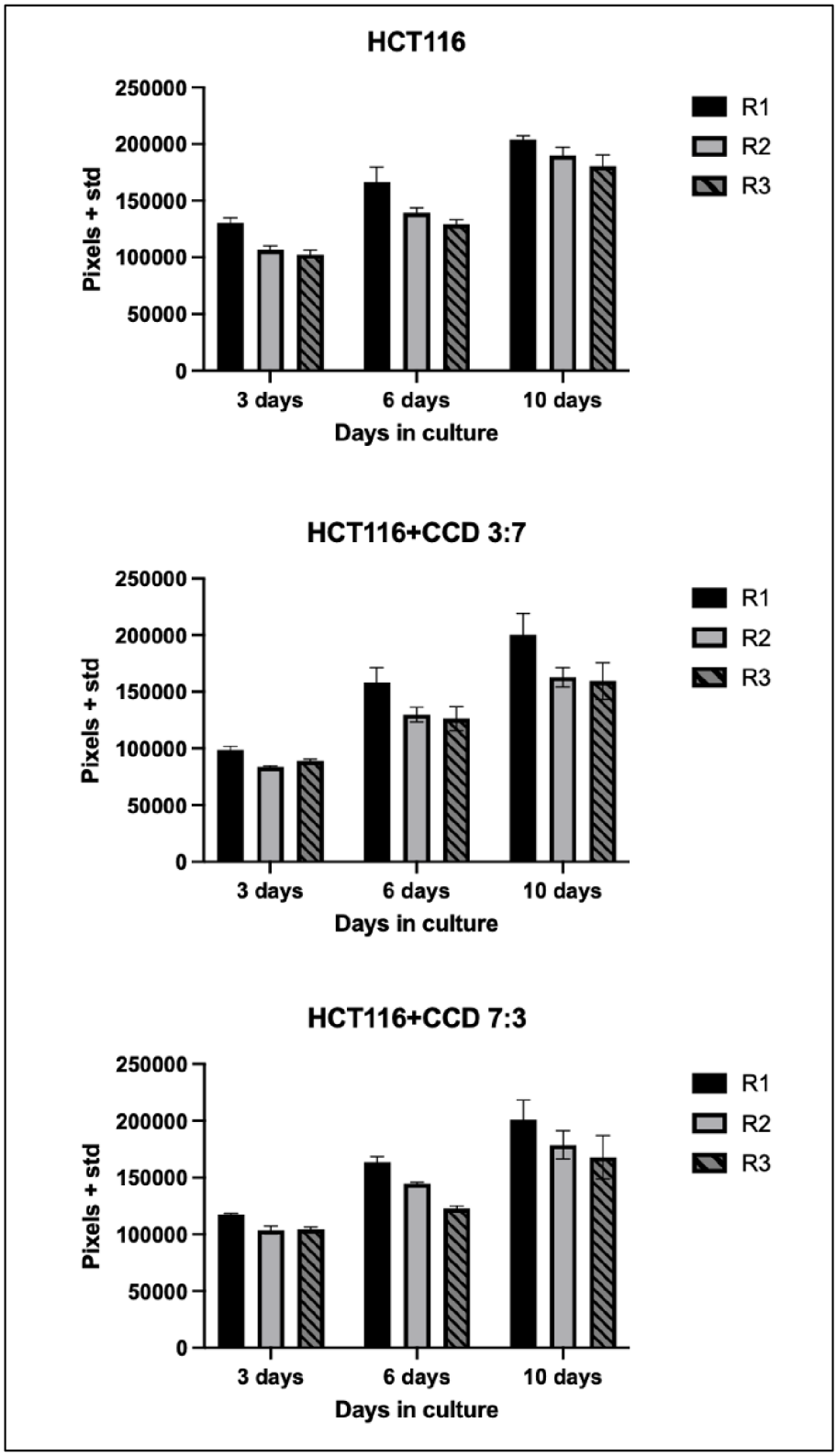

Figure 5.1: Optimization of 3D cell cultivation. Bar graphs of (A) HCT116 monoculture, (B) HCT116 and CCD-18Co coculture at a 3:7 cell ratio (3 HCT116 : 7 CCD-18Co) and (C) HCT116 and CCD-18Co coculture at a 7:3 cell ratio (7 HCT116 : 3 CCD-18Co) over 10 days in culture. Data are presented as mean ± SD of 12 spheroids per experiment from 3 independent experiments.

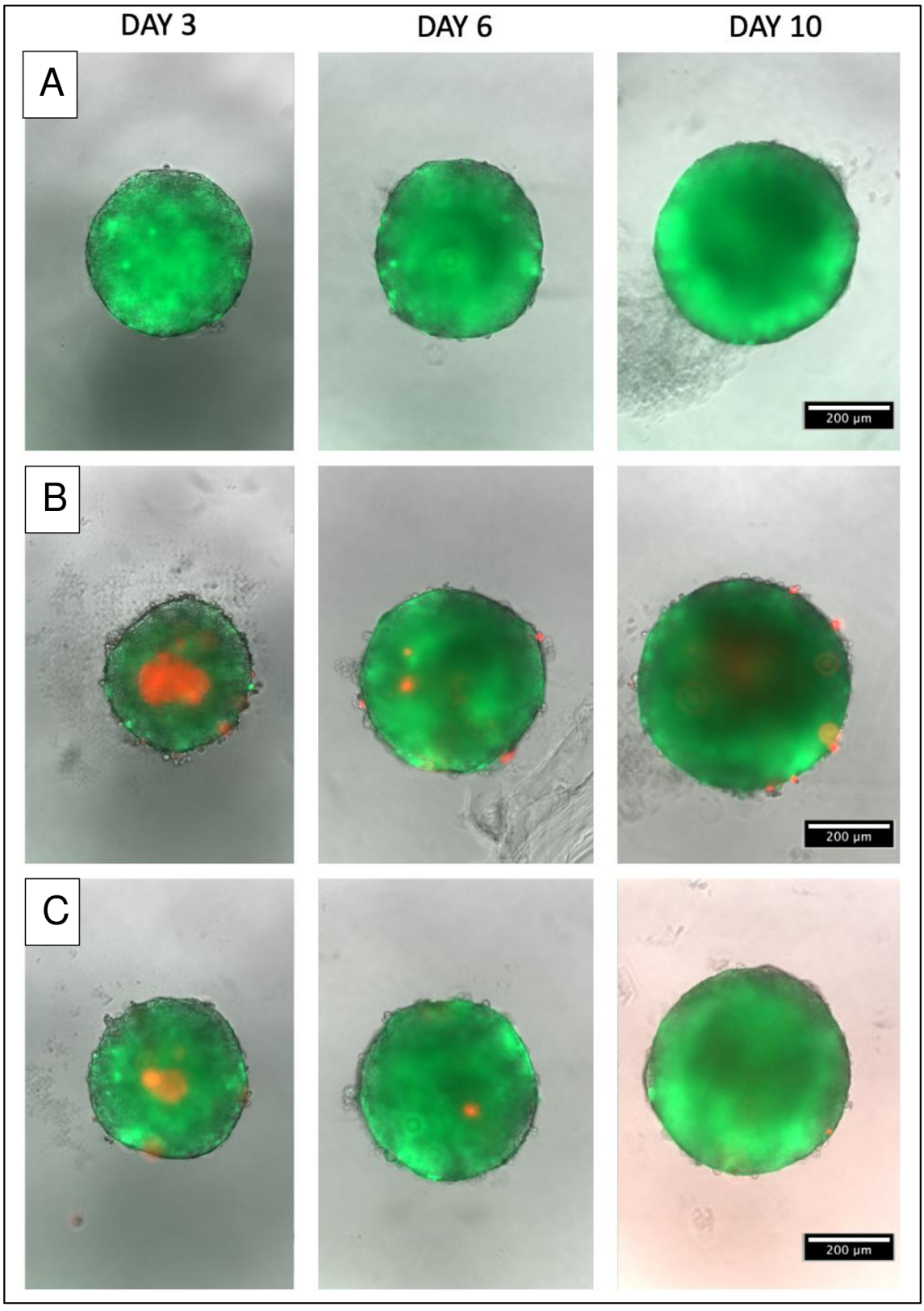

Figure 5.2: Images of (A) HCT116 monoculture, (B) 3:7 HCT116 and CCD-18Co coculture and (C) 7:3 HCT116 and CCD-18Co cocultures spheorids over 10 days in culture. Objective 100×, scale bar 200 µm.

5.2 Single drug treatment of mono- and cocultures

5.2.1 IC_{50} of 5-fluorouracil, irinotecan, and cisplatin

Monocultures and cocultures were treated with 3 different drugs, 5-fluorouracil (5-FU), irinotecan (IR), and cisplatin (CPt), used in the clinic to treat colorectal cancer to obtain the half-maximal inhibitory concentrations (IC_{50}) by CellTiter-Glo® 3D cell viability assay. Each drug was tested at four different concentrations of 1, 20, 50, and 100 µM (4 data points). The experiment was performed four times independently in duplicates for HCT116 monoculture and HCT116 and CCD-18Co cocultures. Treatment lasted for 7 days in total. After 3 days of treatment, the spheroids were imaged using the fluorescent microscope.

Before adding CellTiter-Glo® 3D cell viability assay reagents to treated spheroids, it was important to generate a standard curve for ATP, which determine whether the luminescence produced by the 3D cell cultures is under the 10-µM limit (Figure 5.3) It was obtained calibration curve, which showed increasing luminescence (RFU) in relation to the increasing number of seeded (viable) cells and it was confirmed, that number of cells used for experiment provide ATP content under the 10-µM limit.

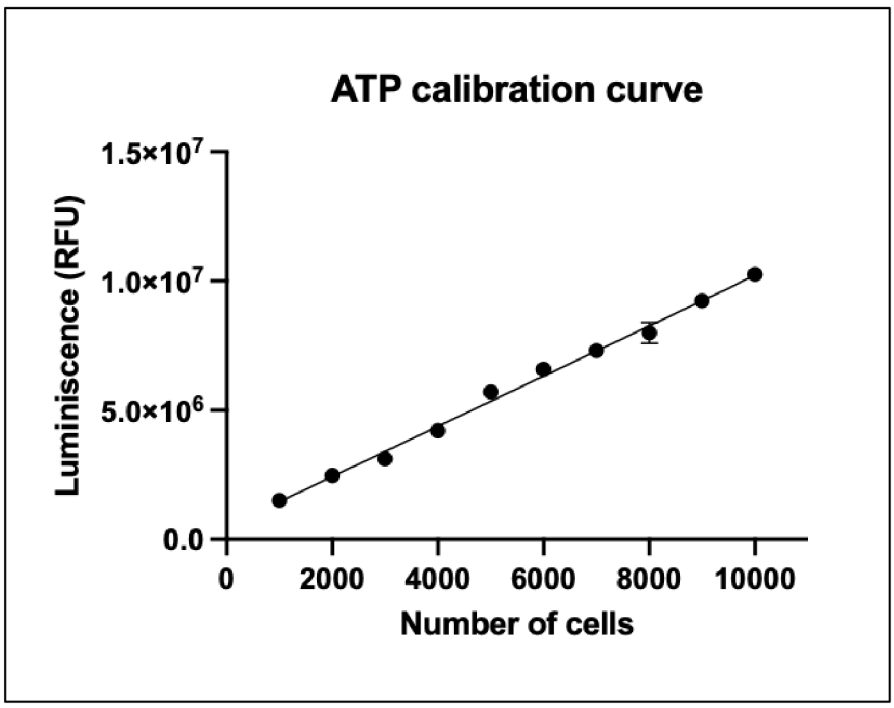

Figure 5.3: ATP standard curve, ATP concentration and cell number correlate with luminescence output.

After confirming that the CellTiter-Glo® 3D cell viability could detect changes in ATP levels in the 3D cultures, spheroids were treated with drugs to determine the IC_{50} concentrations. As shown in Table 5.1, the IC_{50} value of either 5-FU or IR is very similar in monocultures and cocultures, regardless of the cell ratio. The IC_{50} value of 5-FU in HCT116 monoculture was 21.68 ± 5.57 µM, in 3:7 HCT116 and CCD-18Co coculture was 20.20 ± 5.10 µM and in coculture with cell ratio 7:3 it was 23.39 ± 2.93 µM. For IR, the IC_{50} values were also very similar between each culture type. The IC_{50} of IR in HCT116 monoculture was 14.55 ± 8.48 µM, and in cocultures, the IC_{50} was 10.77 ± 2.38 µM for 7:3 cocultures and 3.04 ± 3.34 µM in 7:3 cocultures. Monocultures and cocultures were less sensitive to CPt in general. Interestingly, the IC_{50} value of CPt in HCT116 monoculture is significantly higher than in HCT116 and CCD-18Co cocultures (Figure 5.4). The IC_{50} in HCT116 monocultures was 115.35 ± 32.56 µM, in contrast to cocultures, which were more sensitive to CPt than monocultures. The IC_{50} values in HCT116 and CCD-18Co cocultures with cell ratio 3:7 was 46.20 ± 18.58 µM, and in 7:3 cocultures, it was 42.12 ± 20.14 µM.

Table 5.1: Averaged IC_{50} concentrations (µM) of 5-FU, IR and CPt in HCT116 monocultures and 3:7 and 7:3 HCT116 and CCD-18Co cocultures. Data are mean ± SD from 4 different experiments.

	HCT116	**3:07**	**7:03**
5-FU	21.68 ± 5.57	20.20 ± 5.10	23.39 ± 2.93
IR	14.55 ± 8.48	10.77 ± 2.38	13.04 ± 3.34
CPt	115.35 ± 32.56	46.20 ± 18.58	42.12 ± 20.14

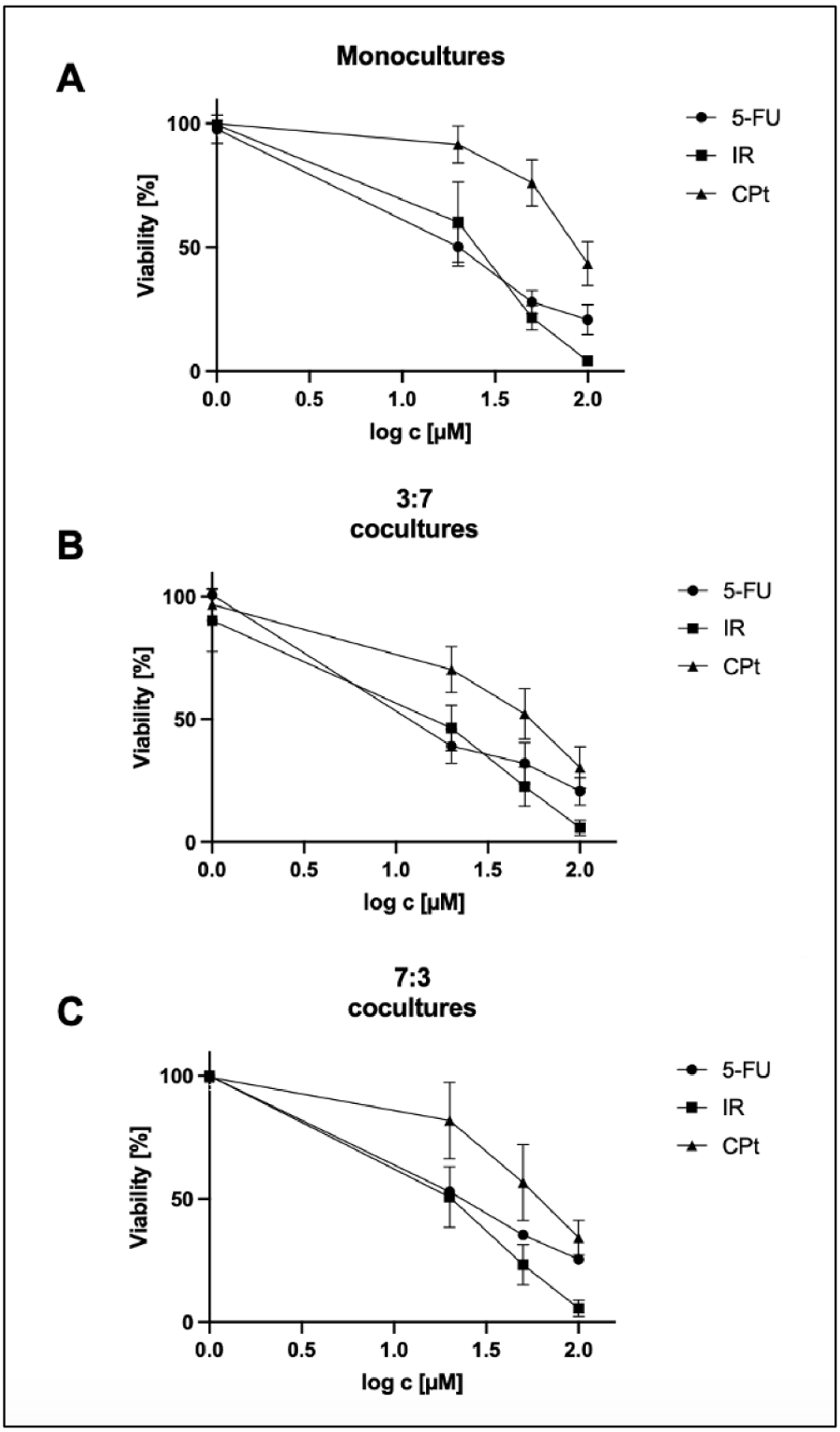

Figure 5.4: Dose-response curves demonstrating the effect of 5-FU, IR and CPt on the viability of HCT116 monoculture spheroids (A), 3:7 HCT116 and CCD-18Co coculture spheroids (B) and 7:3 HCT116 and CCD-18Co coculture spheroids (C). Data are presented as size in pixels ± SD from 3 different experiments.

5.2.2 Imaging of single-drug treatment

HCT116 monocultures and HCT116 and CCD-18Co cocultures were imaged on day 7 following treatment with 5-FU, IR and CPt at concentrations 1, 20, 50, and 100 µM to determine changes in spheroid structure and size. The change in the size of spheroids is summarized in Figure 5.8. A loss of spheroid size in relation to increasing drug concentration can be observed in both monocultures and cocultures.

It can be seen in Figure 5.5 that the size of spheroids was changing with respect to an increase in 5-FU and IR concentration, and thus, with increasing drug concentration, there was a decrease in the size of spheroids. Morphological changes were significant in spheroids treated with IR and 5-FU, and this is evident from the disintegration of spheroids. Changes in spheroids treated with CPt were not remarkable. There was a small change in size, corresponding with the high IC_{50} concentration of CPt in HCT116 monocultures.

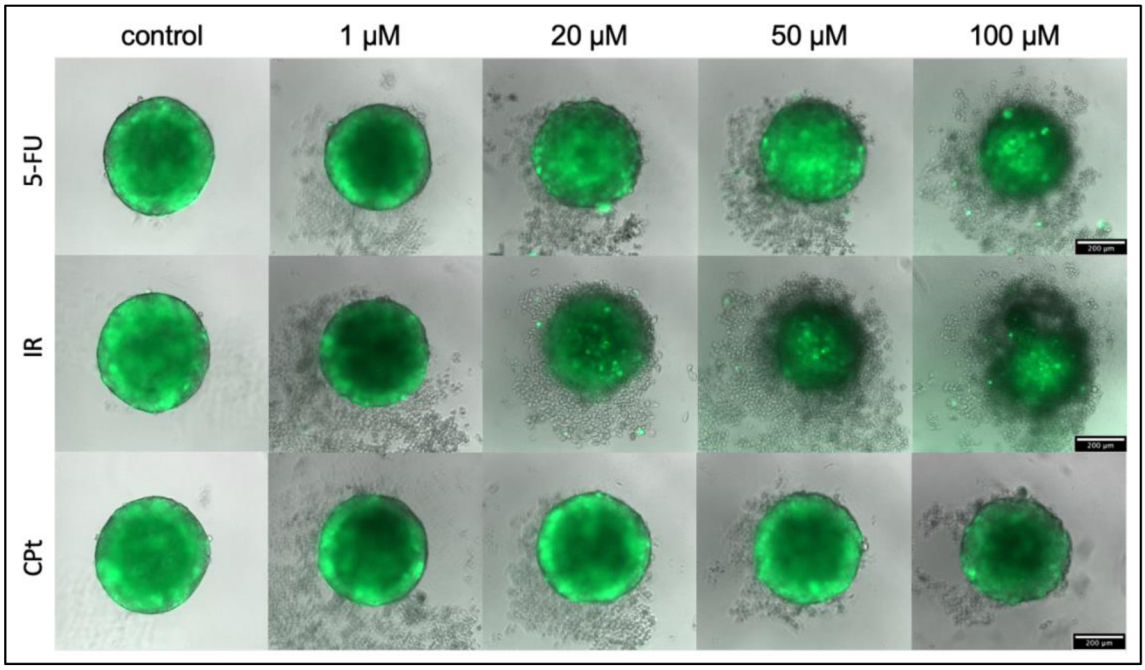

Figure 5.5: Morphological changes in HCT116 monoculture spheroids treated with 5-FU, IR and CPt with the indicated concentrations for 7 days. Objective 100×. Scale bar 200 µm.

Cocultures of HCT116 and CCD-Co18 showed a similar trend as seen following the treatment of monoculture spheroids of HCT116 cells. The circular shape of spheroids was disrupted at the highest concentration of 5-FU and IR, and a loss of GFP signal could be observed clearly. However, there was a robust dsRED2 signal in the CCD-Co18 cells. The changes in CPt-treated spheroids were not that significant; nevertheless, a shrinking of spheroid could be noted. The presence of dead cells without fluorescence signals around spheroids is noted (see Figure 5.6).

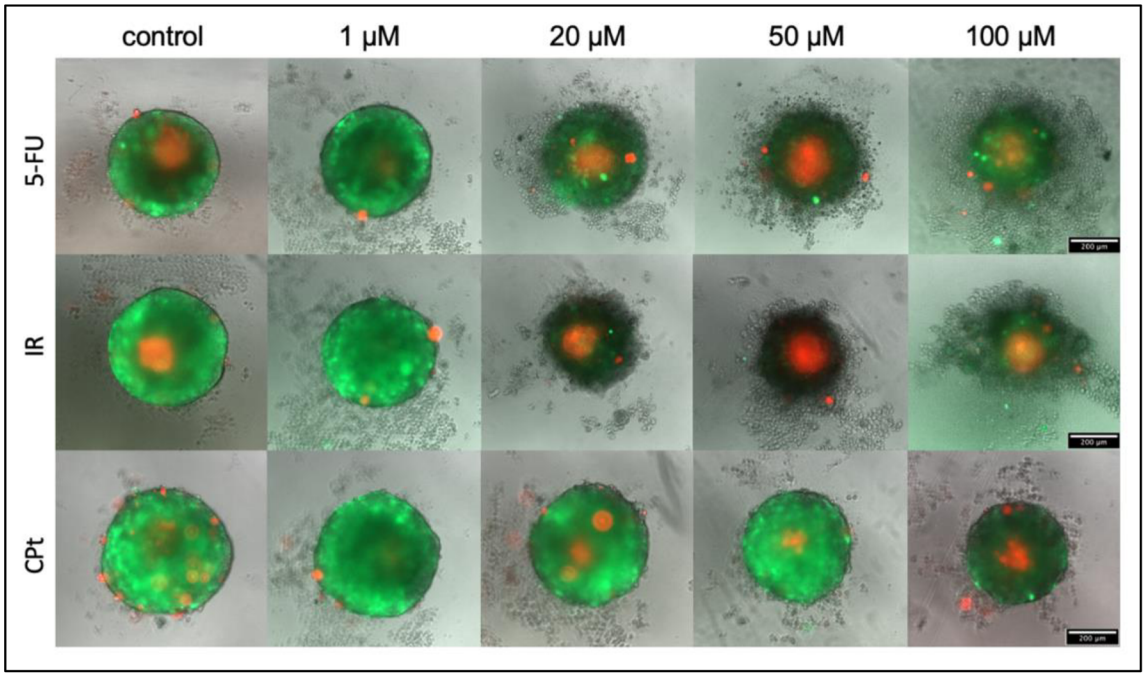

Figure 5.6: Morphological changes in 3:7 coculture spheroids of HCT116 and CCD-18Co cocultures following treatment with 5-FU, IR and CPt for 7 days. The concentrations of drugs were 1, 20, 50 and 100 µM. Objective 100×. Scale bar 200 µm.

A similar effect of drugs was observed in coculture spheroids of HCT116 and CCD-18Co cocultures at a cell ratio of 7:3 (see Figure 5.7) Although spheroids contained fewer CCD-18Co cells than 3:7 coculture spheroids, the dsRED2 signal in spheroids treated with higher concentrations of drugs is greater and localized to the centre. At the highest concentration of 5-FU and IR, the structure of spheroids was significantly disrupted. However, in CPt-treated cells, there were more minor changes in the size of spheroids, as seen in HCT116 monocultures and cocultures with CCD-18Co. Around spheroids, dead cells without signal could be seen, exceptionally cells with either green or red signal, which implies viable cells producing fluorescence color.

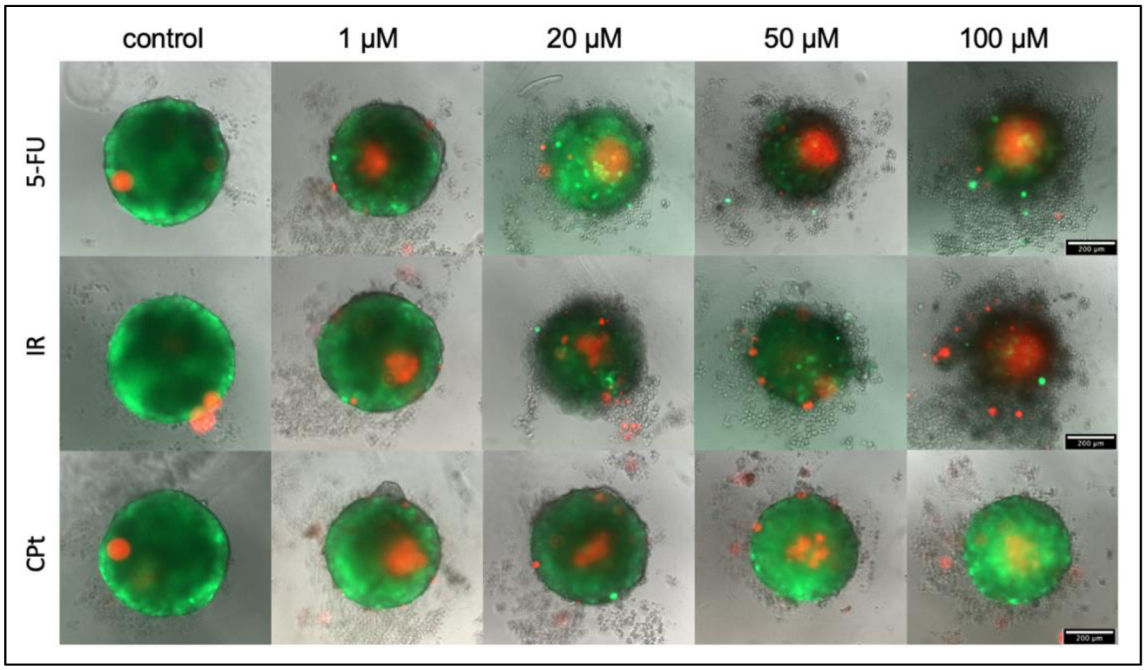

Figure 5.7: Morphological changes in 7:3 coculture spheroids of HCT116 and CCD-18Co cocultures following treatment with 5-FU, IR and CPt for 7 days. The concentrations of drugs were 1, 20, 50 and 100 μM. Objective 100×. Scale bar 200 μm.

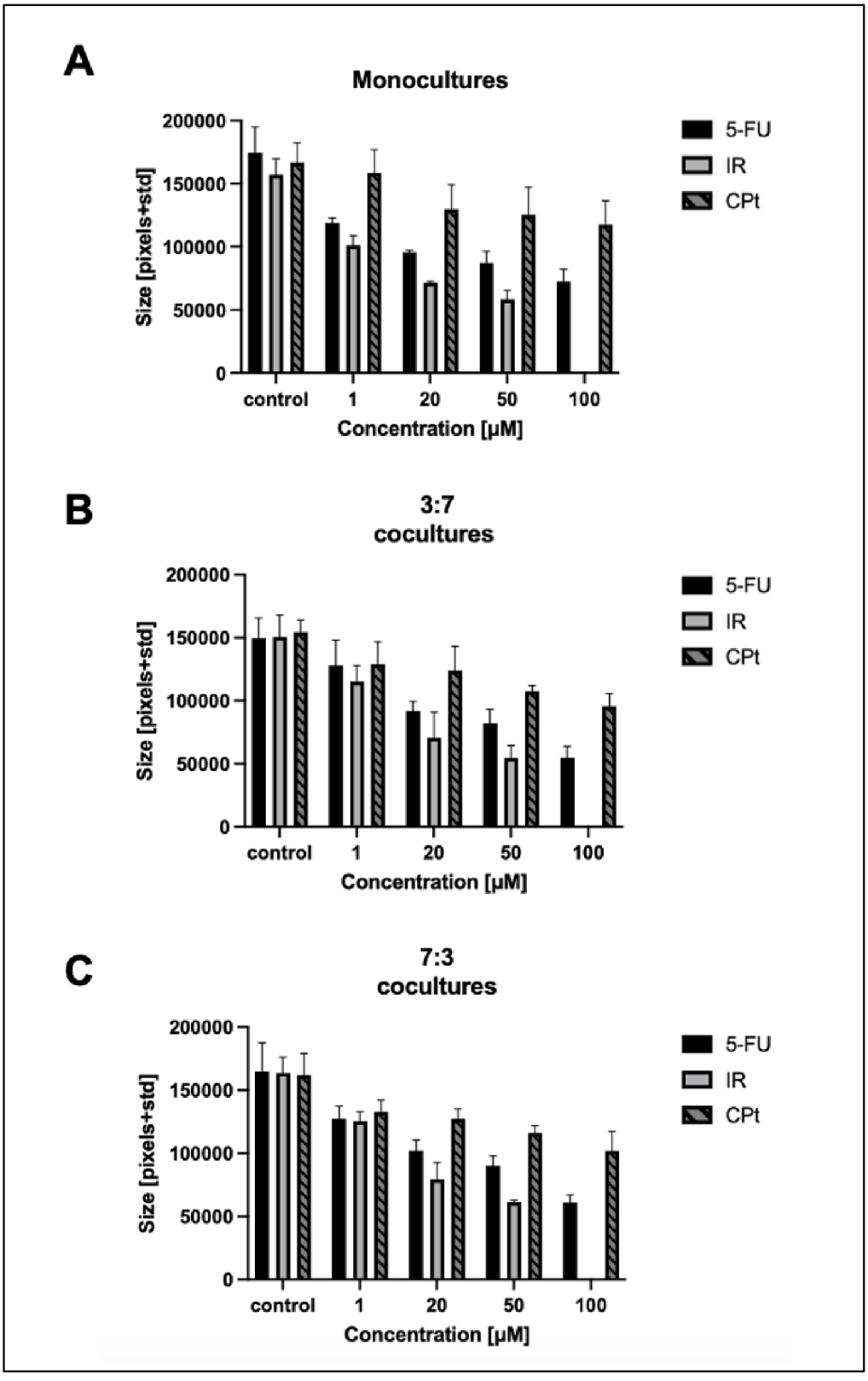

Figure 5.8: Bar graphs of spheroid size changes in (A) HCT116 monoculture, (B) 3:7 HCT116 and CCD-18Co coculture and (C) 7:3 HCT116 and CCD-18Co coculture in response to 5-FU, IR and CPt treatment. Data are presented as size in pixels ± SD from 3 different experiments.

5.3 Drug synergy in mono- and cocultures spheroids

5.3.1 Combination of 5-FU, IR and CPt

The drug combination used for predicting synergy was 5-FU with CPt, and IR with CPt, which are often used in the clinical treatment of cancer; however, noteworthy, CPt showed lower efficiency alone in spheroids. The concentrations of drugs used for the combination study are listed in Table 5.2. Since the IC_{50} values of each drug were very similar in mono- and cocultures, the concentration of drugs for combination treatment was used at a similar range. The only exception was CPt in HCT116 monoculture because the IC_{50} was significantly higher than the IC_{50} of CPt in cocultures. For measuring drug synergy, it is important to treat cells with a concentration of drug that was not higher than the IC_{50} value. Thus, the highest concentration used in the prediction of drug synergy was 20 µM for 5-FU, 12 µM for IR, 110 µM for CPt in HCT116 monoculture and 44 µM for CPt in cocultures. The highest concentration is denoted as 4 and diluted using 2-fold dilution, so the final concentration was 10 µM for 5-FU µM, 6 µM for IR, 55 µM for CPt in monocultures and 22 µM for CPt in cocultures, with the mark 2 in Table 5.2. With the next dilution, the used concentrations were 5 µM for 5-FU, 3 µM for IR, 27.5 µM for CPt in monocultures and 11 µM for CPt in cocultures, and this dilution was marked as 1. Next, spheroids were treated with the following combination ratios – 4:1, 2:1, 1:1, 1:2, 1:4, 5-FU and CPt or IR and CPt.

Table 5.2: Drug concentrations used for their final combination (µM)

Mark	5-FU [µM]	IR [µM]	CPt_{HCT} [µM]	$CPt_{HCT+CCD}$ [µM]
1	5	3	27.5	11
2	10	6	55	22
4	20	12	110	44

5.3.2 Calculation of combination index (CI) using CompuSyn 1.0

The program Compusyn was used to predict the combination index (CI) based on the Chou-Talalay method (see Chapter 4.5.5). Different assay outputs such as spheroid size using microscopy and viability using CellTiter-Glo® 3D Cell Viability Assay were used for calculating CI. Results are summarized in Figures 5.15 and 5.16.

In monocultures, treatment with different combinations of 5-FU, IR and CPt showed synergistic effects (CI < 1). In Table 5.3, the cell viability data shows that the most potent combination in monocultures was 1:1 for 5-FU and CPt, with a combination index 0.29 ± 0.06. The combination of IR and CPt at different drug ratios was not significantly distinct. The most potent drug ratio was 4:1 and 1:4. The value of the combination index was 0.40. The spheroid size data showed that the 5-FU and CPt combination at 1:4 and 1:1 ratios in monoculture spheroids resulted in the highest synergistic effect (CI was 0.34 ± 0.12 for 1:4 combination, and 0.38 ± 0.15 for 1:1 combination). In the case of IR and CPt, the combination at 1:4 ratio showed the highest synergistic effect (CI = 0.21 ± 0.07).

Table 5.3: Combination index of 5-FU and CPt or IR and CPt treatment in HCT116 monocultures. Data are mean ± SD from 3 different experiments.

	Cell viability		**Spheroid size**	
	5-FU:CPt	IR:CPt	5-FU:CPt	IR:CPt
4:1	0.48 ± 0.28	**0.40** ± 0.18	0.48 ± 0.14	0.49 ± 0.10
2:1	0.39 ± 0.07	0.43 ± 0.28	0.66 ± 0.18	0.49 ± 0.13
1:1	**0.29** ± 0.06	0.42 ± 0.29	0.38 ± 0.15	0.32 ± 0.09
1:2	0.50 ± 0.01	0.46 ± 0.24	0.48 ± 0.16	0.25 ± 0.05
1:4	0.50 ± 0.10	**0.40** ± 0.11	**0.34** ± 0.12	**0.21** ± 0.07

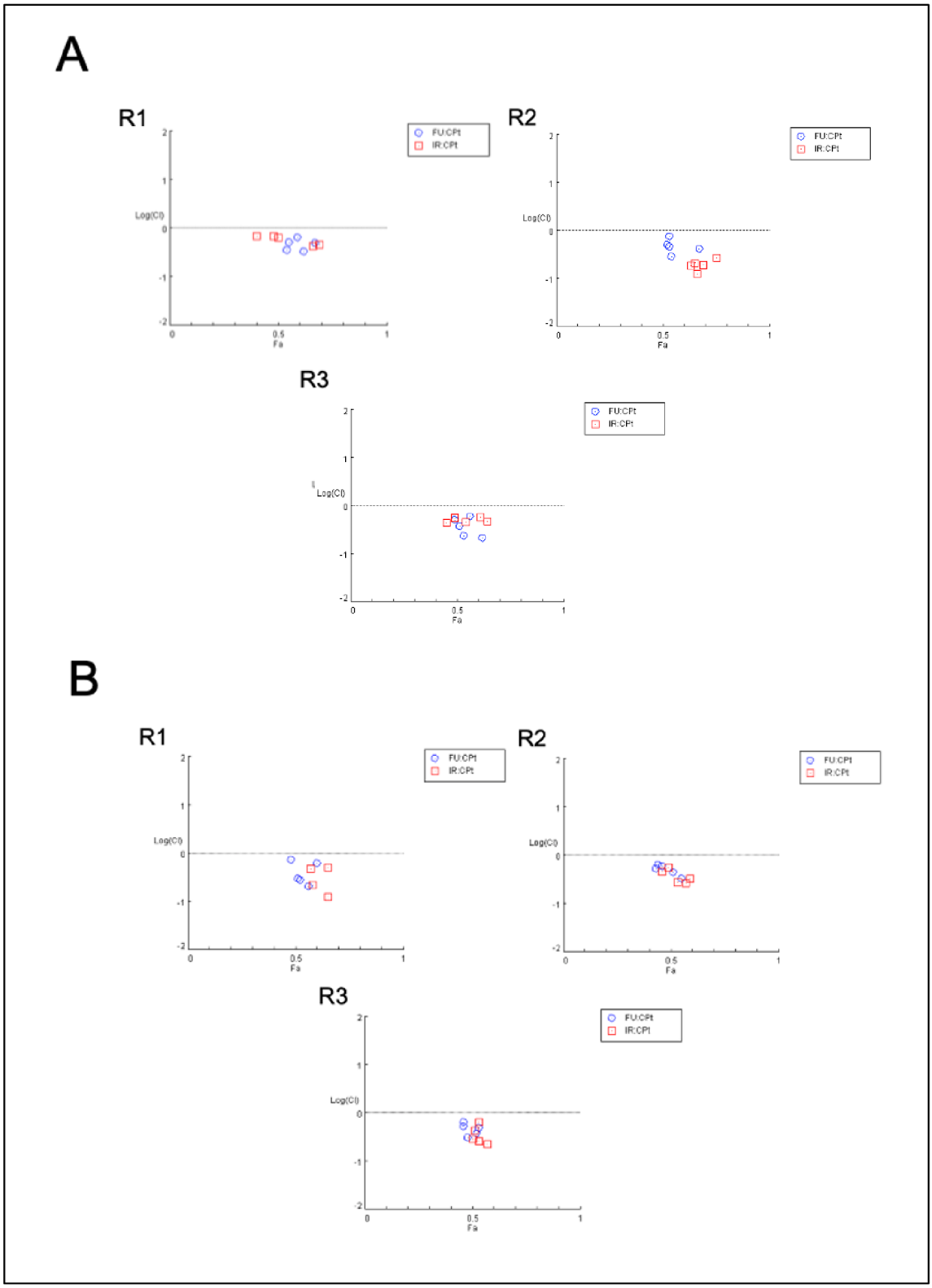

Figure 5.9: Combination index (CI) analysis – fraction affected (Fa) in versus log CI were generated using the method Chou-Talalay to determine the extent of the synergy of 5-FU+CPt and IR+CPt combination in HCT116 monocultures using different parameters such as cell viability (A) and changes in spheroid size (B) in 3 different repeats.

Cell viability data of HCT116 and CCD-18Co cocultures at a ratio of 3:7 showed synergistic effects (CI < 1); however, 5-FU and CPt at 4:1 and 2:1 combination ratios showed faint synergistic effects to additive effects (CI = 1), in combination 4:1 was CI = 0.80 ± 0.32 and 2:1 CI = 0.99 ± 0.53, and their combination is not that efficient when combined. The combination of IR and CPt at a ratio of 1:4 was also showed almost additive effects (CI = 0. 83 ± 0.10). The lowest CI was for 5-FU and CPt at 1:1 (CI = 0.40 ± 0.07) or 1:2 (CI = 0.41 ± 0.06) combination ratios, as in HCT116 monocultures, and 4:1 combination of IR and CPt, when CI was 0.37 ± 0.13. Spheroid size data showed that the most potent ratio of 5-FU and CPt combination was 4:1 (CI = 0.40 ± 0.08), however, cell viability results showed that it is one of the least effective combinations. The CI value of the 1:1 ratio of IR and CPt was 0.40 ± 0.18.

Table 5.4: Combination index of 5-FU and CPt or IR and CPt treatment in HCT116 and CCD-18Co cocultures at a cell ratio of 3:7. Data are mean ± SD from 3 different experiments.

	Cell viability		**Spheroid size**	
	5-FU:CPt	IR:CPt	5-FU:CPt	IR:CPt
4:1	0.80 ± 0.32	**0.37** ± 0.13	**0.40** ± 0.08	0.46 ± 0.13
2:1	0.99 ± 0.53	0.38 ± 0.09	0.43 ± 0.23	0.53 ± 0.14
1:1	**0.40** ± 0.07	0.44 ± 0.05	0.72 ± 0.24	**0.40** ± 0.18
1:2	0.41 ± 0.06	0.54 ± 0.15	0.54 ± 0.20	0.47 ± 0.10
1:4	0.63 ± 0.04	0.83 ± 0.10	0.57 ± 0.26	0.64 ± 0.10

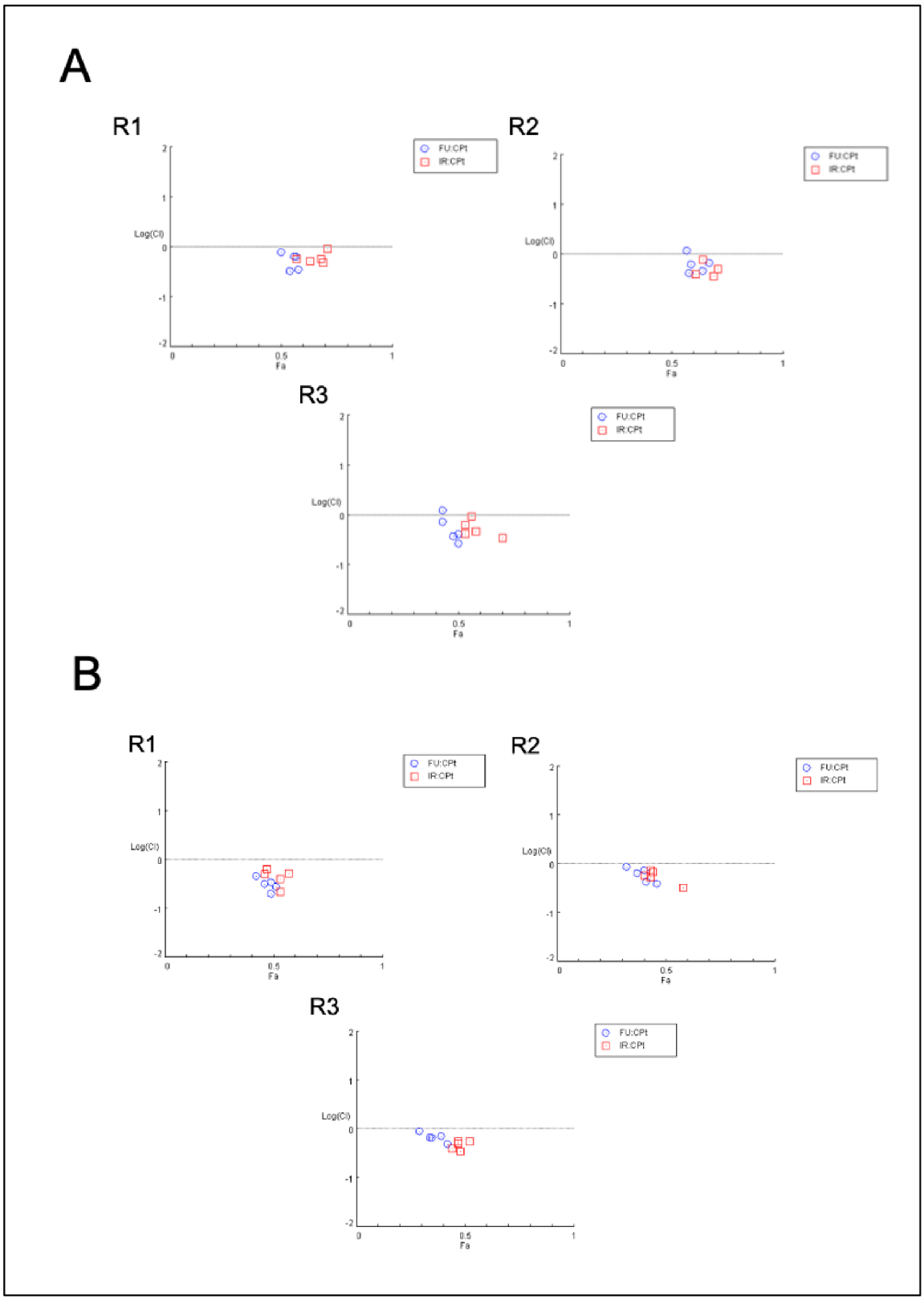

Figure 5.10: Combination index (CI) analysis – fraction affected (Fa) in versus to log CI were generated using the method Chou-Talalay to determine the extent of the synergy of 5-FU+CPt and IR+CPt combination in 3:7 cocultures in 3 repeats and using different parameters such as cell viability (A) and changes in spheroid size (B).

Cell viability data of cocultures at a cell ratio of 7:3 demonstrated a low synergistic effect for 5-FU and CPt. Drug ratio of 1:2 was the most efficient (CI = 0.68 ± 0.11) combination. The spheroid size data showed that the 1:1 combination was (CI = 0.41 ± 0.06); however, CI value significantly differed. The combination of IR and CPt in a 4:1 ratio showed to be the most potent in the cell viability assay (CI = 0.25 ± 0.17), whereas the spheroid size assay also had a similar result (CI = 0.28 ± 0.04). The IR and CPt at a 1:4 combination ratio also showed lower synergistic effects as in 3:7 cocultures.

Table 5.5: Combination index of 5-FU and CPt or IR and CPt treatment in HCT116 and CCD-18Co cocultures at a cell ratio of 7:3. Data are mean ± SD from 3 different experiments.

	Cell viability		**Spheroid size**	
	5-FU:CPt	IR:CPt	5-FU:CPt	IR:CPt
4:1	0.94 ± 0.08	**0.25** ± 0.17	0.43 ± 0.08	**0.28** ± 0.04
2:1	0.78 ± 0.28	0.31 ± 0.18	0.57 ± 0.11	0.30 ± 0.13
1:1	0.74 ± 0.12	0.32 ± 0.09	**0.41** ± 0.06	0.44 ± 0.10
1:2	**0.68** ± 0.11	0.49 ± 0.17	0.44 ± 0.13	0.41 ± 0.12
1:4	0.84 ± 0.14	0.72 ± 0.23	0.56 ± 0.06	0.46 ± 0.11

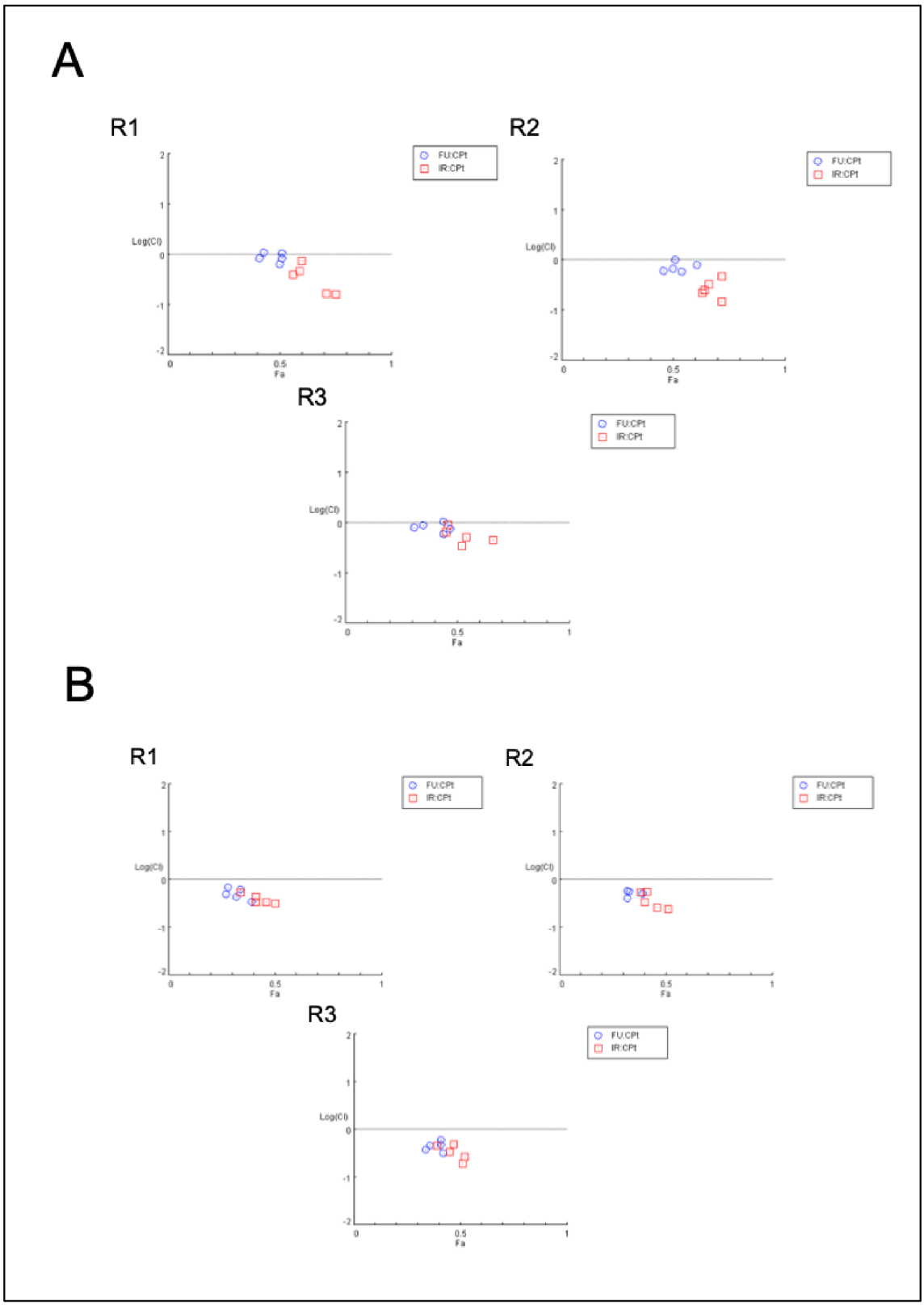

Figure 5.11: Combination index (CI) analysis – fraction affected (Fa) in versus to log CI were generated using the method Chou-Talalay to determine the extent of the synergy of 5-FU+CPt and IR+CPt combination in 7:3 cocultures in 3 repeats and using different parameters such as cell viability (A) and changes in spheroid size (B).

5.3.3 Imaging of spheroids after treatment

Mono- and cocultures were imaged after 7 days of treatment to observe their size and fluorescence signal changes. Spheroids were treated with a combination of 5-FU and CPt or IR and CPt at ratios 4:1, 2:1, 1:1, 1:2 and 1:4 or with a single drug at concentrations that corresponded to that in the combination (Table 5.2). In treated mono- and cocultures, disruption of spheroids and the release of dead cells from spheroid to the surroundings can be observed. Imaging showed, that the most effective was treatment with IR (see Figures 5.12, 5.13 and 5.14) either alone (A) or combined with CPt (B) and had the same effect in mono- and cocultures. It could be observed changes in spheroid structure in relation to increasing drug concentration and apoptotic cells in spheroid surroundings. Also, the size of spheroids changes in response to different drug combinations compared to control untreated cells.

In cocultures with a cell ratio of 3:7, it can be seen that CCD-18Co dsRED2 cells are located in the centre of spheroids (Figure 5.13). In 7:3 cocultures containing fewer CCD-18Co cells, the dsRED2 signal could be seen throughout the spheroids (Figure 5.14). The percentage of viability and changes in spheroids size are summarized in Figures 5.15 and 5.16. Viability and size of spheroid decreased about hald compared to control cells.

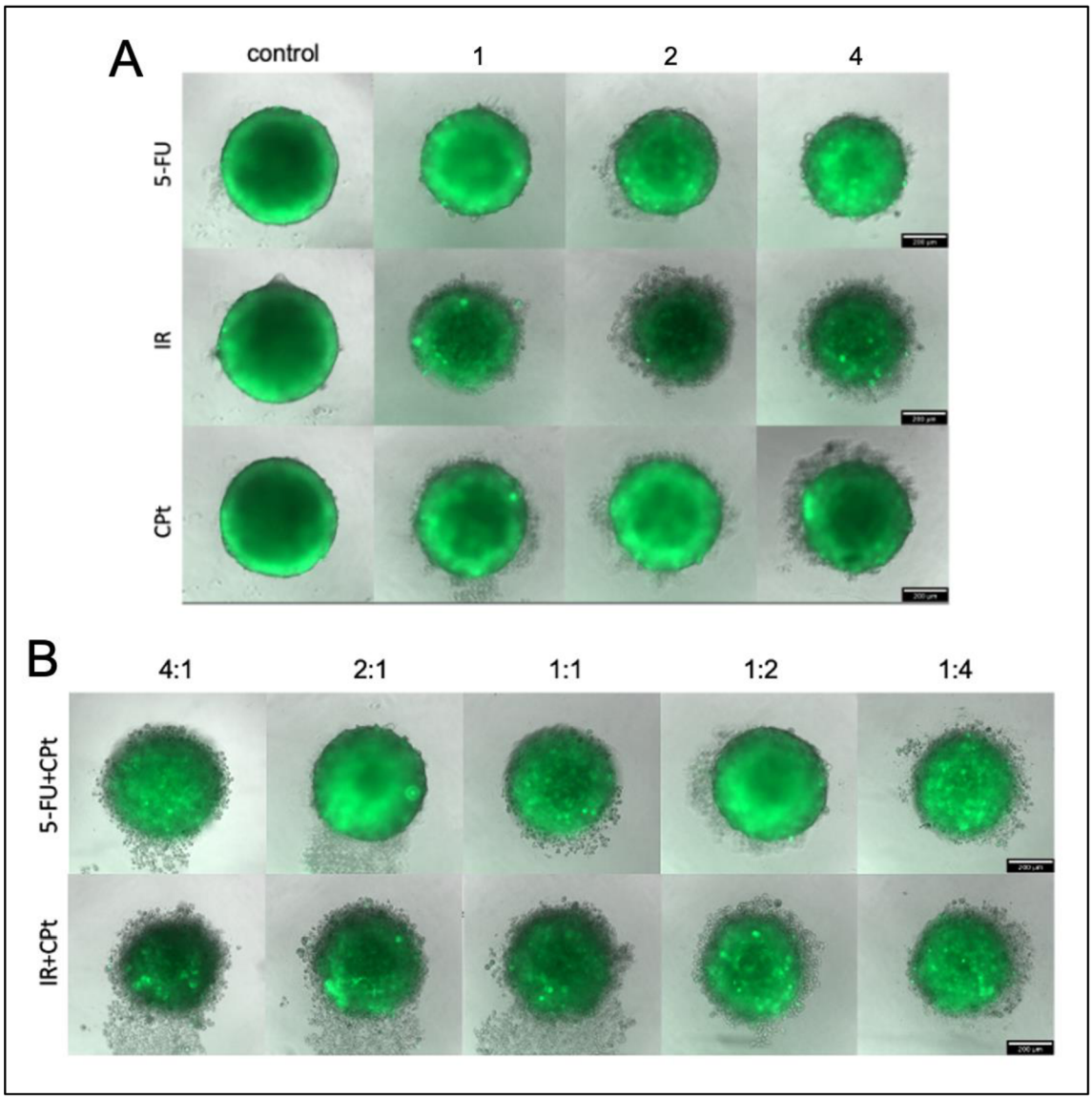

Figure 5.12: Morphological changes in HCT116 monocultures after single drug treatment with 5-FU, IR and CPt (A) and combination treatment with 5-FU and CPt or IR and CPt at different ratios (B). Objective 100×. Scale bar 200 µm.

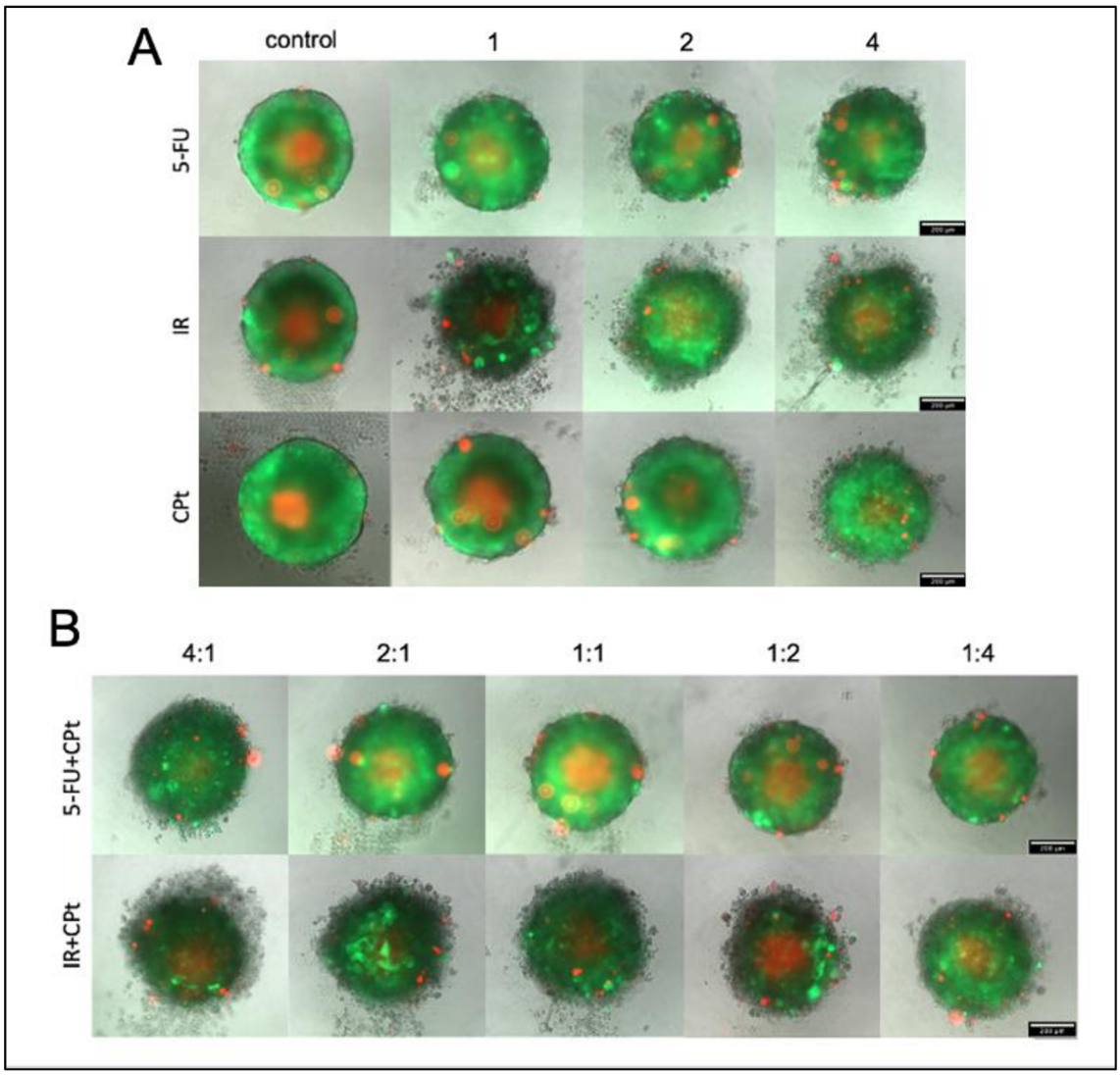

Figure 5.13: Morphological changes in HCT116 and CCD-18Co cocultures at a cell ratio of 3:7 after single drug treatment with 5-FU, IR and CPt (A) and following treatment with combination 5-FU and CPt or IR and CPt at different ratios (B). Phase-contrast photomicrographs with GFP and dsRED2 signal are shown. Objective 100×. Scale bar 200 µm.

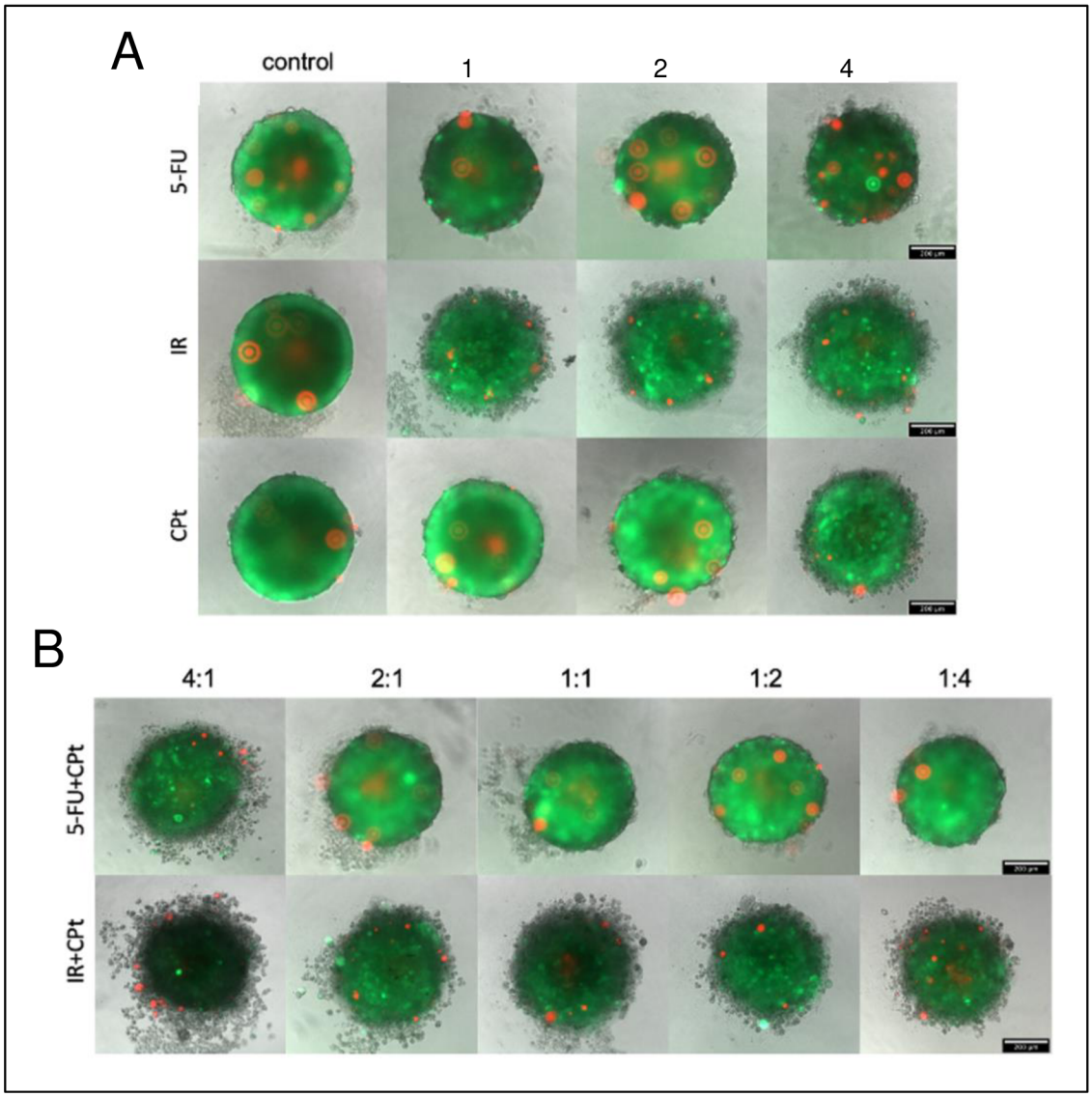

Figure 5.14: Morphological changes in HCT116 and CCD-18Co cocultures at a cell ratio of 7:3 after single drug treatment with 5-FU, IR and CPt (A) and following treatment with combination 5-FU and CPt or IR and CPt at different ratios (B). Phase-contrast photomicrographs with GFP and dsRED2 signal are shown. Objective 100×. Scale bar 200 µm.

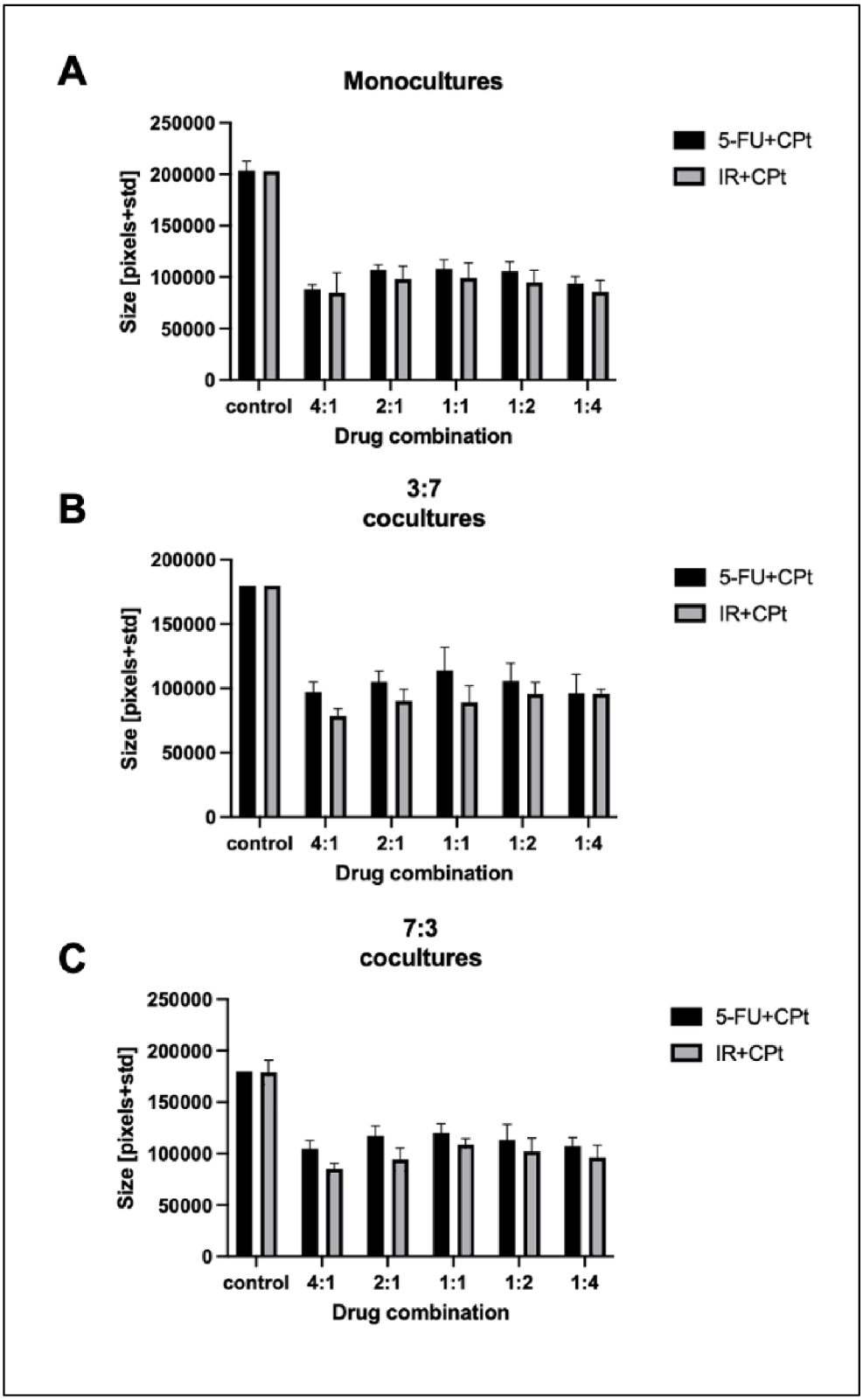

Figure 5.15: Bar graphs of spheroid size change in (A) HCT116 monoculture, (B) HCT116 and CCD-18Co coculture at 3:7 cell ratio and (C) HCT116 and CCD-18Co coculture at 7:3 cell ratio in response to 5-FU, IR and CPt treatment. Data are presented as size in pixels ± SD from 3 different experiments.

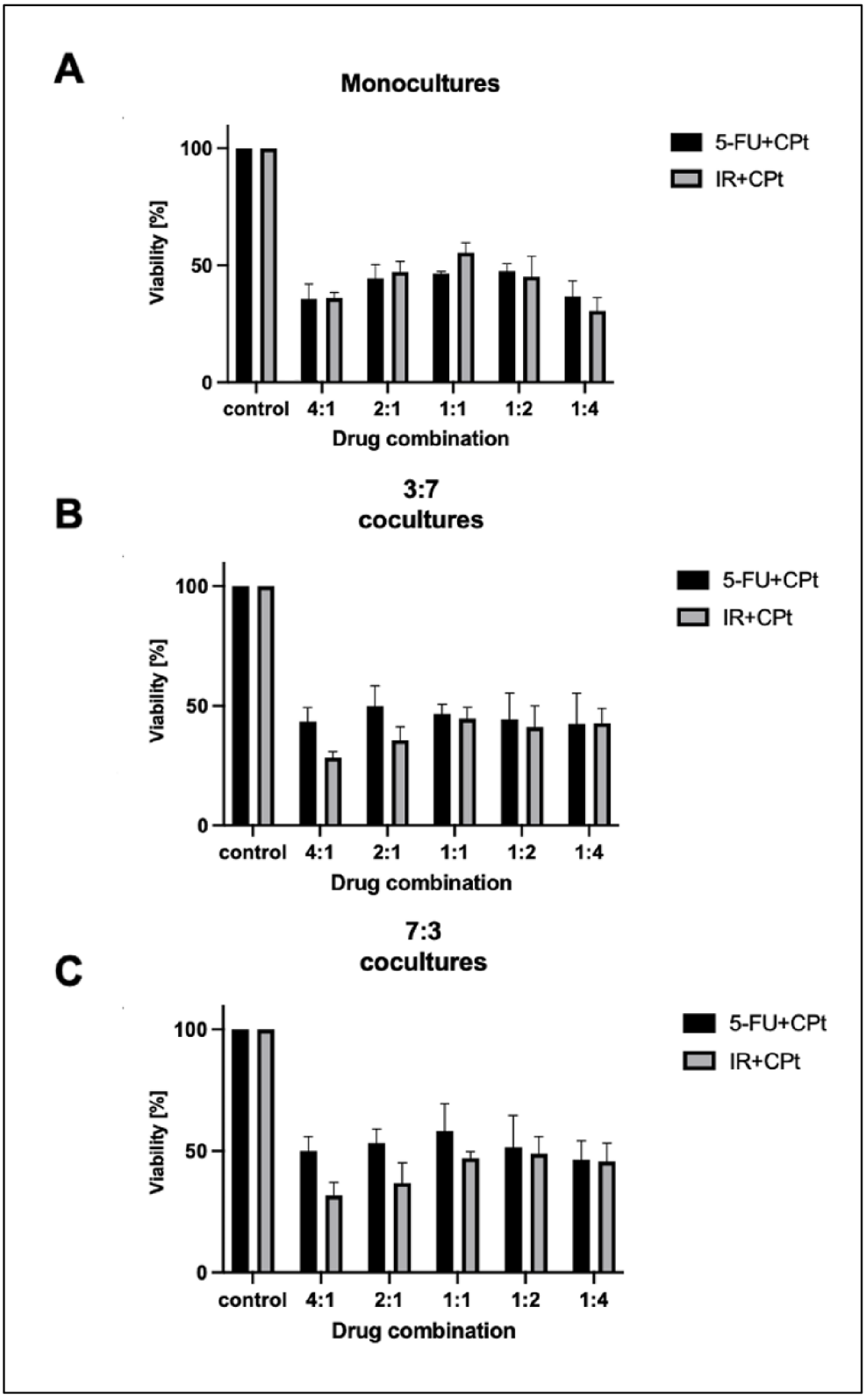

Figure 5.16: Bar graphs of the viability of (A) HCT116 monoculture, (B) HCT116 and CCD-18Co coculture at 3:7 cell ratio and (C) HCT116 and CCD-18Co coculture at 7:3 cell ratio in response to 5-FU, IR and CPt treatment. Data are presented as viability in mean ± SD of 3 different experiments.

6 DISCUSSION

In this study, 3 types of 3D cell cultures – HCT116 monocultures, HCT116 and CCD-18Co cocultures at two ratios of 3:7 and 7:3 at a density 5 000 cells/well in agarose-coated plates were successfully prepared. Spheroids were observed, and their size was measured until day 10 to monitor their continuous growth over time. After optimizing and obtaining uniform-sized spheroids (approximately) in each experiment, single-drug treatment with 5-FU, IR, and CPt, clinically used to treat colorectal cancer, was performed.

Single drug treatment showed that IR is a very potent drug compared to 5-FU and CPt, which was expected since it is used as the second-line therapy for colorectal cancer (Mármol *et al.*, 2017). 5-FU also showed great efficacy in both mono- and cocultures; however, the IC_{50} of cisplatin was significantly different in mono- and cocultures. CPt was less potent in monoculture, and IC_{50} was two times higher. Thus, it was necessary to treat monocultures with higher doses of cisplatin than in cocultures for further drug combinations. This can be explained by the lower sensitivity of HCT116 cell culture to cisplatin, whereas HCT116 cell content in cocultures was lower than in monocultures, and thus, the sensitivity was higher.

Two parameters were used to predict synergy in mono- and cocultures – cell viability and spheroid size. Combining IR with CPt showed synergistic effects in mono- and cocultures; however, cell viability data showed that 5-FU and CPt treated spheroids have low synergistic to additive effects when combined at ratios 4:1 and 2:1. This was not the case in spheroid size data. Cell viability data showed that cocultures were less responsive to the combination of 5-FU with CPt, and 1:4 combination of IR and CPt, than monocultures. This may have resulted due the presence of CCD-18Co fibroblast cells, mimicking stroma cells in tumors and affecting drug response (Zoetemelk *et al.*, 2018). Activated fibroblasts can result in changed proliferation and participate in tumor resistance. They are also involved in changes in tumor neo-angiogenesis, which leads to metastasis (Onfroy-Roy *et al.*, 2021).

CI values differed between methods focusing on different parameters, i.e., cell viability and spheroid size. Also, spheroid response to drug treatment differed between experiments, which can be caused by deviation in size, proliferation rate,

and hypoxic conditions in spheroids, affecting ATP production. Hypoxia downregulates ATP production (Wheaton et Chandel, 2011), which is the basis of the CellTiter-Glo® 3D Cell Viability Assay Kit. Despite ambiguous results of synergy study between changes in cell viability and spheroid size, single-drug treatment of spheroids showed an effective response.

3D cultures can replicate natural tumor architecture, with proliferating zone, internal zone with limited oxygen, nutrient and growth factor distribution, hypoxic and necrotic core, which significantly influence drug responses. The spheroid size can be easily controlled by cell density number, making 3D cultures very promising for further use in cancer drug development. However, with the advantages come disadvantages, such as reproducibility problems and variabilities between different models (Barbosa *et al.*, 2022). Cells in 3D cultures can show differential sensitivity according to the cultivation methods used for generating 3D cultures and unstable culture conditions that influence metabolic activity and cell proliferation (Imamura *et al.*, 2015). Next, in CRC, the distinguishing factor affecting tumor development, progression, suppression of immune response and others is the presence of cancer-associated fibroblasts through secretion of different molecules mediating tumor-stroma crosstalk. Compared to 2D cultures, 3D cultures showed lower sensitivity to some drugs. 2D cultures face many disadvantages, such as not mimicking a tumor microenvironment or lack of cell-cell or cell-stroma interactions, which influence drug response and lack of physiologically relevant hypoxia environment and variable metabolic pathways, making the correlation of data from 2D culture cumbersome for clinical use (Griffith *et* Swartz, 2006).

7 CONCLUSION

The 3D cultures have the potential to become an important model for preclinical studies aimed at developing new cancer drugs by significantly reducing drug failures. The thesis aimed to generate HCT116 monocultures and cocultures of HCT116 and CCD-18Co cells using agarose-coated plates for testing their potential use for drug synergy assays. This was tested using 3 clinical drugs, 5-FU, IR and CPt, alone or in combination on different assay parameters, such as spheroid size using microscopy and viability.

Data show that the combination of 5-FU with CPt and IR with CPt has synergistic effects in both mono- and cocultures based on changes in spheroid size. However, cell viability data suggests low synergistic to additive effects of some combinations of 5-FU and CPt in cocultures due to the presence of CCD-18Co fibroblasts. Conversely, synergy data generated using changes in spheroid size showed synergistic effects of the same combination in cocultures. Responses to IR and CPt combination were similar in mono- and cocultures. Values of CI differed between used methods, so it is important to use different methods to confirm results for drug development.

The 3D cultures can effectively mimic the microtumor environment, and the drug response results and further synergy studies can be more relevant in the development of cancer drugs. Therefore, it is important to focus on developing 3D culture systems and studying the effects of different treatments using these systems.

8 REFERENCES

Agrawal, Khushboo, Viswanath Das, Pankhuri Vyas, and Marián Hajdúch. 2018. "Nucleosidic DNA demethylating epigenetic drugs – A comprehensive review from discovery to clinic". 188: 45-79.

Arnold, Christian N., Ajay Goel, Hubert E. Blum, and C. Richard Boland. 2005. "Molecular pathogenesis of colorectal cancer". *Cancer* 104: 2035-2047.

Barbosa, Mélanie A. G., Cristina P. R. Xavier, Rúben F. Pereira, Vilma Petrikaitė, and M. Helena Vasconcelos. 2022. "3D Cell Culture Models as Recapitulators of the Tumor Microenvironment for the Screening of Anti-Cancer Drugs". *Cancers* 14.

Boland, C. Richard, and Ajay Goel. 2010. "Microsatellite Instability in Colorectal Cancer". *Gastroenterology* 138: 2073-2087

Bonnans, Caroline, Jonathan Chou, and Zena Werb. 2014. "Remodelling the extracellular matrix in development and disease". *Nature Reviews Molecular Cell Biology* 15: 786-801.

Breslin, Susan, and Lorraine O'Driscoll. 2013. "Three-dimensional cell culture: the missing link in drug discovery". *Drug Discovery Today* 18 (5-6): 240-249.

Cushing, Melinda C., and Kristi S. Anseth. 2007. "Hydrogel Cell Cultures". *Science* 316 (5828): 1133-1134.

Dasari, Shaloam, and Paul Bernard Tchounwou. 2014. "Cisplatin in cancer therapy: Molecular mechanisms of action". *European Journal of Pharmacology* 740: 364-378.

Das, Viswanath, Francesca Bruzzese, Petr Konečný, Federica Iannelli, Alfredo Budillon, and Marián Hajdúch. 2015. "Pathophysiologically relevant in vitro tumor models for drug screening". *Drug Discovery Today* 20 (7): 848-855.

Das, Viswanath, Tomáš Fürst, Soňa Gurská, Petr Džubák, and Marián Hajdúch. 2016. "Reproducibility of Uniform Spheroid Formation in 384-Well Plates". *SLAS Discovery* 21 (9): 923-930.

Fearon, Eric R. 1995. "Molecular Genetics of Colorectal Cancer". *Annals of the New York Academy of Sciences* 768 (1): 101-110.

Fearon, Eric R., and Bert Vogelstein. 1990. "A genetic model for colorectal tumorigenesis". *Cell* 61 (5): 759-767.

Ferlay, Jacques, Murielle Colombet, Isabelle Soerjomataram, Donald M. Parkin, Marion Piñeros, Ariana Znaor, and Freddie Bray. 2021. "Cancer statistics for the year 2020: An overview". *International Journal of Cancer* 149 (4): 778-789.

Ferreira, L.P., V.M. Gaspar, and J.F. Mano. 2018. "Design of spherically structured 3D in vitro tumor models -Advances and prospects". *Acta Biomaterialia* 75: 11-34.

Foglietta, Federica, Loredana Serpe, and Roberto Canaparo. 2021. "The Effective Combination between 3D Cancer Models and Stimuli-Responsive Nanoscale Drug Delivery Systems". *Cells* 10 (12).

Folkesson, Evelina, Barbara Niederdorfer, Vu To Nakstad, Liv Thommesen, Geir Klinkenberg, Astrid Lægreid, and Åsmund Flobak. 2020. "High-throughput screening reveals higher synergistic effect of MEK inhibitor combinations in colon cancer spheroids". *Scientific Reports* 10 (1).

Gilazieva, Zarema, Aleksei Ponomarev, Catrin Rutland, Albert Rizvanov, and Valeriya Solovyeva. 2020. "Promising Applications of Tumor Spheroids and Organoids for Personalized Medicine". *Cancers* 12 (10).

Goldberg, Richard M., Daniel J. Sargent, Roscoe F. Morton, Charles S. Fuchs, Ramesh K. Ramanathan, Stephen K. Williamson, Brian P. Findlay, Henry C. Pitot, and Steven R. Alberts. 2004. "A Randomized Controlled Trial of Fluorouracil Plus Leucovorin, Irinotecan, and Oxaliplatin Combinations in Patients With Previously Untreated Metastatic Colorectal Cancer". *Journal of Clinical Oncology* 22 (1): 23-30.

Grady, William M., and John M. Carethers. 2008. "Genomic and Epigenetic Instability in Colorectal Cancer Pathogenesis". *Gastroenterology* 135 (4): 1079-1099.

Greco WR, Bravo G, Parsons JC. 1995. "The search for synergy: a critical review from a response surface perspective". *Pharmacol Rev.* Jun; 47 (2): 331-85.

Griffith, Linda G., and Melody A. Swartz. 2006. "Capturing complex 3D tissue physiology in vitro". *Nature Reviews Molecular Cell Biology* 7 (3): 211-224.

Haycock, John W. 2011. "3D Cell Culture: A Review of Current Approaches and Techniques". *Methods Mol Biol.*: 1-15.

Hickman, John A., Ralph Graeser, Ronald de Hoogt, Suzana Vidic, Catarina Brito, Matthias Gutekunst, Heiko van der Kuip, and IMI PREDECT consortium. 2014. "Three-dimensional models of cancer for pharmacology and cancer cell biology: Capturing tumor complexity in vitro/ex vivo". *Biotechnology Journal* 9 (9): 1115-1128.

Hirschhaeuser, Franziska, Heike Menne, Claudia Dittfeld, Jonathan West, Wolfgang Mueller-Klieser, and Leoni A. Kunz-Schughart. 2010. "Multicellular tumor spheroids: An underestimated tool is catching up again". *Journal of Biotechnology* 148 (1): 3-15.

Chou, Ting-Chao. 2010. "Drug Combination Studies and Their Synergy Quantification Using the Chou-Talalay Method". *Cancer Research* 70 (2): 440-446.

Chou, Ting-Chao. 2006. "Theoretical Basis, Experimental Design, and Computerized Simulation of Synergism and Antagonism in Drug Combination Studies". *Pharmacological Reviews* 58 (3): 621-681.

Chou, Ting-Chao, and Paul Talalay. 1983. "Analysis of combined drug effects: a new look at a very old problem". *Trends in Pharmacological Sciences* 4: 450-454.

Imamura, Y., T. Mukohara, Y. Shimono, Y. Funakoshi, N. Chayahara, M. Toyoda, N. Kiyota, et al. 2015. "Comparison of 2D- and 3D-culture models as drug-testing platforms in breast cancer". *Oncology Reports* 33 (4): 1837-1843.

Jemal, Ahmedin, Freddie Bray, Melissa M. Center, Jacques Ferlay, Elizabeth Ward, and David Forman. 2011. "Global cancer statistics". *CA: A Cancer Journal for Clinicians* 61 (2): 69-90.

Jensen, Caleb, and Yong Teng. 2020. "Is It Time to Start Transitioning From 2D to 3D Cell Culture?". *Frontiers in Molecular Biosciences* 7 (March).

Lancaster, Madeline A, and Juergen A Knoblich. 2014. "Generation of cerebral organoids from human pluripotent stem cells". *Nature Protocols* 9 (10): 2329-2340.

Langhans, Sigrid A. 2018. "Three-Dimensional in Vitro Cell Culture Models in Drug Discovery and Drug Repositioning". *Frontiers in Pharmacology* 9 (January).

Lao, Victoria Valinluck, and William M. Grady. 2011. "Epigenetics and colorectal cancer". 8 (12): 686-700.

Laurent, Jennifer, Céline Frongia, Martine Cazales, Odile Mondesert, Bernard Ducommun, and Valérie Lobjois. 2013. "Multicellular tumor spheroid models to explore cell cycle checkpoints in 3D". *BMC Cancer* 13 (1).

Lv, Donglai, Shi-cang Yu, Yi-fang Ping, Haibo Wu, Xilong Zhao, Huarong Zhang, Youhong Cui, et al. 2016. "A three-dimensional collagen scaffold cell culture system for screening anti-glioma therapeutics". *Oncotarget* 7 (35): 56904-56914.

Mármol, Inés, Cristina Sánchez-de-Diego, Alberto Pradilla Dieste, Elena Cerrada, and María Rodriguez Yoldi. 2017. "Colorectal Carcinoma: A General Overview and Future Perspectives in Colorectal Cancer". *International Journal of Molecular Sciences* 18 (1).

Onfroy-Roy, Lauriane, Dimitri Hamel, Laurent Malaquin, and Audrey Ferrand. 2021. "Colon Fibroblasts and Inflammation: Sparring Partners in Colorectal Cancer Initiation?". *Cancers* 13 (8).

Palmer, Adam C., and Peter K. Sorger. 2017. "Combination Cancer Therapy Can Confer Benefit via Patient-to-Patient Variability without Drug Additivity or Synergy". *Cell* 171 (7): 1678-1691.e13.

Pino, Maria S., and Daniel C. Chung. 2010. "The Chromosomal Instability Pathway in Colon Cancer". *Gastroenterology* 138 (6): 2059-2072.

Sauer, Rolf, Heinz Becker, Werner Hohenberger, Claus Rödel, Christian Wittekind, Rainer Fietkau, Peter Martus, et al. 2004. "Preoperative versus Postoperative Chemoradiotherapy for Rectal Cancer". *New England Journal of Medicine* 351 (17): 1731-1740.

Shi, Si, Wantong Yao, Jin Xu, Jiang Long, Chen Liu, and Xianjun Yu. 2012. "Combinational therapy: New hope for pancreatic cancer?". *Cancer Letters* 317 (2): 127-135.

Straussman, Ravid, Teppei Morikawa, Kevin Shee, Michal Barzily-Rokni, Zhi Rong Qian, Jinyan Du, Ashli Davis, et al. 2012. "Tumour micro-environment elicits innate resistance to RAF inhibitors through HGF secretion". *Nature* 487 (7408): 500-504.

Sung, Hyuna, Jacques Ferlay, Rebecca L. Siegel, Mathieu Laversanne, Isabelle Soerjomataram, Ahmedin Jemal, and Freddie Bray. 2021. "Global Cancer Statistics 2020: GLOBOCAN Estimates of Incidence and Mortality Worldwide for 36 Cancers in 185 Countries". *CA: A Cancer Journal for Clinicians* 71 (3): 209-249.

Tallarida, R. J. 2012. "Quantitative Methods for Assessing Drug Synergism". 2 (11): 1003-1008.

Van Cutsem, E., A. Cervantes, B. Nordlinger, and D. Arnold. 2014. "Metastatic colorectal cancer: ESMO Clinical Practice Guidelines for diagnosis, treatment and follow-up". *Annals of Oncology* 25: iii1-iii9.

Wheaton, William W., and Navdeep S. Chandel. 2011. "Hypoxia. 2. Hypoxia regulates cellular metabolism". *American Journal of Physiology-Cell Physiology* 300 (3): C385-C393.

Zafar, S. Yousuf, and Hirsch. "Capecitabine in the management of colorectal cancer". *Cancer Management and Research*.

Zanoni, Michele, Filippo Piccinini, Chiara Arienti, Alice Zamagni, Spartaco Santi, Rolando Polico, Alessandro Bevilacqua, and Anna Tesei. 2016. "3D tumor spheroid models for in vitro therapeutic screening: a systematic approach to enhance the biological relevance of data obtained". *Scientific Reports* 6 (1).

Zhao, Liang, M. Guillaume Wientjes, and Jessie L-S Au. 2010. "Comparison of methods for evaluating drug-drug interaction". *Frontiers in Bioscience* E2 (1): 241-249.

Zoetemelk, Marloes, Magdalena Rausch, Didier J. Colin, Olivier Dormond, and Patrycja Nowak-Sliwinska. 2019. "Short-term 3D culture systems of various complexity for treatment optimization of colorectal carcinoma". *Scientific Reports* 9 (1).